




Polar metals taxonomy for materials classification and discovery

Daniel Hickox-Young ^{*}, Danilo Puggioni [†], and James M. Rondinelli [‡]

Department of Materials Science and Engineering, Northwestern University, Evanston, Illinois 60208, USA



(Received 10 October 2022; accepted 22 December 2022; published 9 January 2023)

Over the past decade, materials that combine broken inversion symmetry with metallic conductivity have gone from a thought experiment to one of the fastest growing research topics. In 2013, the observation of the first uncontested polar transition in a metal, LiOsO_3 , inspired a surge of theoretical and experimental work on the subject, uncovering a host of materials which combine properties previously thought to be contraindicated [Shi *et al.*, *Nat. Mater.* **12**, 1024 (2013)]. As is often the case in a nascent field, the sudden rise in interest has been accompanied by diverse (and sometimes conflicting) terminology. Although “ferroelectriclike” metals are well defined in theory, i.e., materials that undergo a symmetry-lowering transition to a polar phase while exhibiting metallic electron transport, real materials find a myriad of ways to push the boundaries of this definition. Here, we review and explore the burgeoning polar metal frontier from the perspectives of theory, simulation, and experiment while introducing a unified taxonomy. The framework allows one to describe, identify, and classify polar metals; we also use it to discuss some of the fundamental tensions between theory and models of reality inherent in the terms “ferroelectric” and “metals.” In addition, we highlight shortcomings of electrostatic doping simulations in modeling different subclasses of polar metals, noting how the assumptions of this approach depart from experiment. We include a survey of known materials that combine polar symmetry with metallic conductivity, classified according to the mechanisms used to harmonize those two orders and their resulting properties. We conclude by describing opportunities for the discovery of novel polar metals by utilizing our taxonomy.

DOI: [10.1103/PhysRevMaterials.7.010301](https://doi.org/10.1103/PhysRevMaterials.7.010301)

I. INTRODUCTION

The concept of crystalline metals without inversion symmetry, specifically those that lift parity symmetry to support a polar crystal structure, has been frequently attributed to a concise 1965 paper by Blount and Anderson [1]. What is less well appreciated is that Blount and Anderson’s paper focuses on how a nominally first-order *ferroelastic* transition, observed at the time in the metallic silicide V_3Si , could exhibit second-order character, presumably attributed to a displacive component akin to the paraelectric-to-ferroelectric transition found in insulating compounds, which exhibit a well-defined polarization below the critical temperature. At the time, nearly all martensitic (ferroelastic) transformations in metals exhibited strong first-order character [2]; yet, V_3Si exhibited second-order behavior. The continuous response was rationalized by inferring that the symmetry break should be *like* that found in second-order displacive ferroelectrics, hence the quotes around “ferroelectric” in the title of their paper. Blount and Anderson did not suppose that “ferroelectric” metals would possess a switchable polarization. Gauss’s law dictates that no electric field may exist within a homogeneous metal

[3,4], so the atomic structure of an ideal polar metal should be immune to perturbation via an external applied electric field.

Ironically, for years this same physical law seemed to imply that polar metals should not exist at all. In prototypical ferroelectrics like BaTiO_3 it was shown that the polar displacement was stabilized by long-range dipole-dipole interactions [5,6]. In the presence of free charge carriers, such interactions would be completely screened, favoring the centrosymmetric structure. In the decades following Anderson and Blount’s work, it appeared that Gauss’s law would prevail over the synthesis of a polar metal. There were several candidates in the 2000s which combined polar order and metallicity via compositional ordering, but it was not until 2013 that Shi *et al.* showed the metal LiOsO_3 exhibited a displacive transition [7]. Their work demonstrated that a “ferroelectriclike” transition need not rely on long-range interactions, but may derive from local structural effects (geometrically driven Li displacements in the case of LiOsO_3). The discovery of LiOsO_3 quickly led to work on a theoretical framework for predicting the existence of other metals with a displacive phase transition. Puggioni and Rondinelli outlined several mechanisms through which one might stabilize a polar metal and formulated the weak-coupling hypothesis, which states that the coexistence of polar displacements and metallic conductivity is predicated upon the decoupling of the two orders [8]. The years following the discovery of LiOsO_3 have seen significantly increased interest in polar metals (Fig. 1), further accelerated by the discovery of nontrivial topological metals and their ensuing phenomena and properties [9–11]. During

^{*}Present address: Department of Mathematics, Computer Science and Physics, Roanoke College, Salem, Virginia 24153, USA; hickoxyoung@roanoke.edu

[†]daniло.puggioni@northwestern.edu

[‡]jrondinelli@northwestern.edu

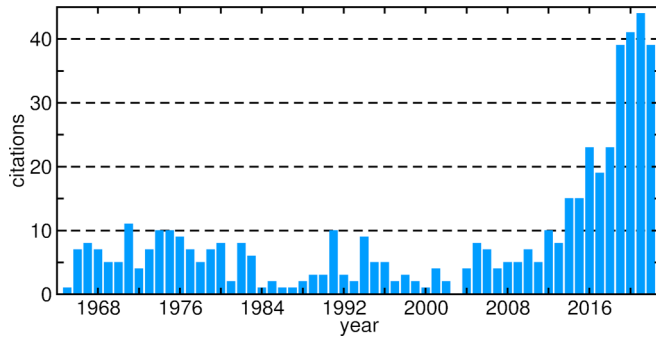


FIG. 1. Citations per year of Anderson and Blount’s 1965 paper on second-order martensitic phase transitions [1]. Data collected from Google Scholar on December 19th, 2022.

the rapid increase in scholarship, diverse methods of combining these previously contraindicated properties have been proposed and executed, ranging from degenerately doped ferroelectrics [12–15] to metals with hybrid improper polar distortions [16,17] to two-dimensional thin films and interfaces [18–20]. Reviews of the classification of different design strategies and detailed microscopic descriptions for some polar metals can be found in Refs. [21–23].

Accompanying these materials are a variety of terms. Polar, ferroelectric, “ferroelectric,” ferroelectriclike, and native ferroelectric are all qualifiers used to describe metallic systems with broken inversion symmetry and unique directions in the crystal. Unique directions are distinct from polar directions in crystals, which are defined such that the two ends are not related via a symmetry operation of the point group. Hence, all unique directions are polar, but not vice versa [24]. Furthermore, many so-called “ferroelectric metals” either push the boundaries of what may be called “metallic” or do not exhibit a switchable polarization. Given the advances in dielectric, modern polarization, and soft-mode theories [25–29], we find that the ferroelectriclike designation and its derivatives [18,30–33] are cumbersome and nonessential descriptions, obfuscating the physics displayed by very different (and yet, equally interesting) classes of materials. In addition, we note that both experimental and computational approaches to studying these materials have at times been abused. Computationally, the background-charge approach to electrostatic doping simulations fails to model reality in multiple underappreciated ways [34,35]. Meanwhile, in experiment, the application of ferroelectric characterization techniques to materials that are not formally ferroelectrics both erode the key differences separating metals from dielectrics and can lead to misinterpretations of measured dielectric polarizations, e.g., electric polarization hysteresis [30,36].

In this work, we propose using meaningful atomic and electronic structure descriptions to distinguish materials based on conductivity and symmetry considerations. We begin by discussing the tensions between theory and experiment, as exemplified by both the various methods for combining polar order and metallicity and the shortcomings of our current terminology. These issues are further amplified in computational studies using electronic structure methods, e.g., with the popular background-charge approach to electrostatic doping

simulations, which can lead to model results inconsistent with experiment. We then present a survey of polar metals classified using our taxonomy that combines conductivity with broken inversion using terminology based on clearly defined class descriptors.

II. TENSIONS IN TERMINOLOGY: “FERROELECTRIC” “METALS”

Between the realms of theory and experiment, communication is critical in order to foster a productive relationship. Since communication is built on having a common vocabulary, this makes the terminology we use of utmost importance in seeking to advance the current understanding of our field and not just a pedantic dilemma. In the field of polar metals, however, some classifiers that seem obvious in theory are less well defined in experiment and the result has been confusing and at times unintentionally misleading. We present a few examples of the two most common sources of dissonance between theoretical and experimental labels, namely, “metallic” and “ferroelectric,” and suggest methods for relieving the tension.

A. Ferroelectric “metals”

How to define metallicity? The question of how one defines a “metal” carries significance for many disciplines, but the distinction bears considerable weight when evaluating doped ferroelectrics (FEs), especially as several reports describe doping known FEs as a route to achieve polar or “ferroelectric” metals. At what point does a doped ferroelectric become a polar metal? Is there an important fundamental difference between a polar structure with intrinsic charge carriers or extrinsic charge carriers? To answer these questions, let us consider fundamental definitions of metallicity.

According to Kohn’s theory, while the wave function of the electrons in a metal in its ground state is delocalized, that of an insulator is localized [37]. This distinction strictly defines the difference between metals and insulators. Electron transport considerations can, in principle, be used to quite clearly separate metals from insulators (dielectrics). According to Mott, “...a metal conducts, and a nonmetal doesn’t” [38,39]. This statement is strictly true at $T = 0$ K and is often used as the discriminating factor between a metal and an insulator (or semiconductor) such that

$$\lim_{T \rightarrow 0} \rho(T) = \begin{cases} \infty & \text{insulator,} \\ \rho_0 & \text{metal,} \end{cases} \quad (1)$$

where ρ corresponds to the electric resistivity of the material and ρ_0 is the residual resistivity due to electron collisions with crystal impurities and imperfections at $T = 0$ K. Importantly, the value of ρ at room temperature does not matter; thus, although the definition is mathematically well defined, experimental conditions ($T \neq 0$ K) can make the differentiation challenging, especially when the carrier density of a semiconductor is sufficiently high at room temperature. These may be intrinsic charge carriers or the result of degenerate doping, such that the material is conductive through extrinsic doping [15,40–42]. These compounds are polar, and for reasonably large temperature ranges there is a positive correlation

between resistivity and temperature, even though (strictly speaking) the correlation between resistivity and temperature becomes negative at low temperature. This fact may be why the boundary between doped polar semiconductors and polar metals is frequently blurred by experiment, despite the clear theoretical distinction [37,43,44].

Band theory. The distinction between a trivial insulator and a metal can be understood using band theory. For an insulator, such as an intrinsic semiconductor, the Fermi level resides in the middle of an energy gap, such that thermal excitations produce equal numbers of electrons and holes as described by Fermi-Dirac statistics. Therefore, at 0 K, there are no free charge carriers available and $\rho \rightarrow \infty$. With increasing temperature, the electrons thermally populate the conduction band and become available for conduction such that the resistivity decreases ($d\rho/dT < 0$). In metals, the Fermi level is located within a band, giving rise to free charge carriers. As temperature increases, so does resistivity ($d\rho/dT > 0$). At high temperatures ($T \gg \Theta_D$, where Θ_D is the Debye temperature), $\rho \sim T$. At low temperatures $T \ll \Theta_D$ and ρ has four contributions [45]

$$\rho(T) = \rho_0 + AT^2 + BT^5 + CT^f \exp\left(-\frac{\hbar\omega_{\min}}{k_B T}\right).$$

The T^2 contribution originates from electron-electron scattering. The T^5 contribution was evaluated by Bloch and Grüniessen [46,47] and is due to electron-phonon scattering. The exponential term describes the contribution of electron-phonon umklapp scattering, where ω_{\min} is the minimum phonon frequency below which umklapp processes are forbidden and f is an empirical parameter. To be considered genuinely metallic, polar metals should exhibit a positive correlation between resistivity and temperature for all $T > 0$ K. This is exactly what happens for LiOsO_3 , which shows Fermi-liquid-like behavior ($\rho \sim T^2$) in its polar phase [7]. With this in mind we can answer the following question: At what point does a doped semiconductor become metallic? The threshold to achieve metallic conductivity is determined by the carrier concentration required to make $d\rho/dT > 0$.

The ratio $d\rho/dT$ is useful for differentiating metals from insulators. However, we note that metallic and insulating phases are limiting situations. In transition metal oxides and other strongly correlated systems, $\rho(T)$ exhibits complex behavior. For instance, the polar oxide $\text{Ca}_3\text{Ru}_2\text{O}_7$ exhibits metallic conductivity above 48 K, insulating behavior from 48 to 30 K, and shows again metallic transport below 30 K [48]. Even doped ferroelectrics exhibit complex transport properties. In La-doped BaTiO_3 , $\rho(T)$ shows insulating behavior from 350 to 260 K, metallic transport between 260 and 70 K, and again insulating behavior with localization below 70 K [41]. Therefore, the assessment of metal and nonmetal status using $d\rho/dT$ alone is not an easy task and should be performed in conjunction with other descriptors.

Drude definition. Although the dc conductivity would appear to be the natural way to separate metals from insulators, in practice assessing the frequency-dependent free-carrier response of a material allows one to treat metals, doped semiconductors, and insulators on more equal footing [50]. For a perfect crystalline material with noninteracting electrons, the

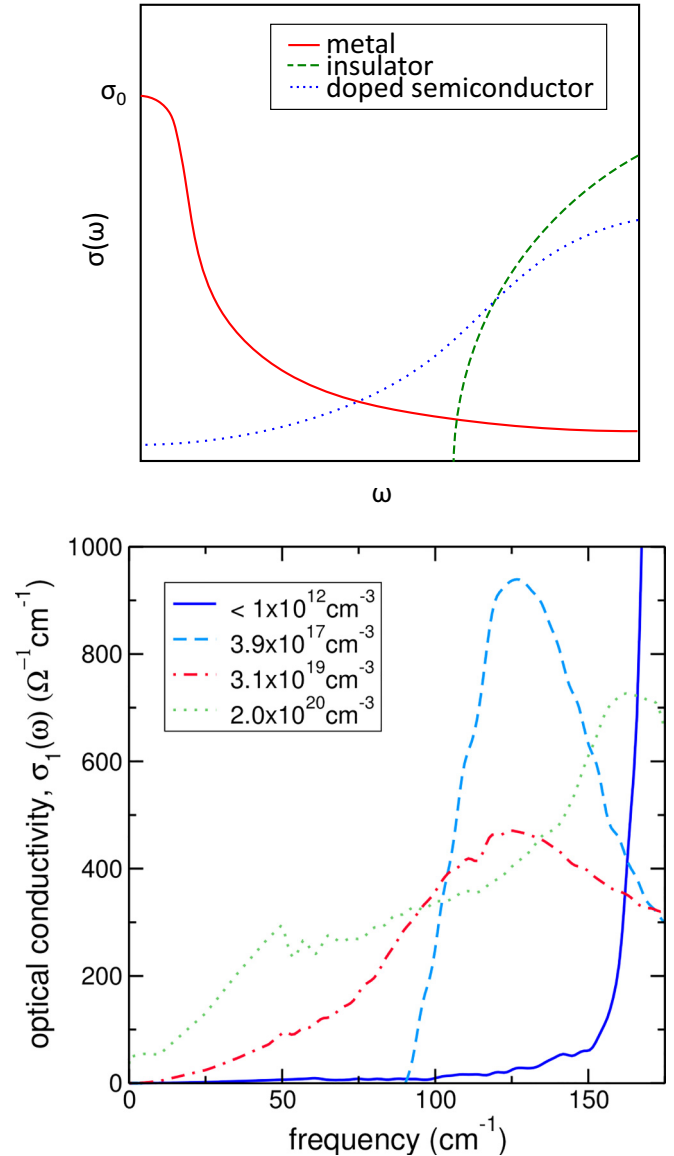


FIG. 2. (Top) Schematic illustration of the difference in optical conductivity responses across materials classes. (Bottom) Experimental data from Ref. [49] illustrating the evolution of the optical conductivity of $\text{BaTiO}_{3-\delta}$ under oxygen vacancy doping at $T \approx 30$ K.

optical conductivity σ relates the electrical current density due to a spatially uniform transverse electric field as

$$\sigma(\omega) = \frac{ne^2\tau}{m(1 - i\omega\tau)},$$

where m is the mass of the carrier (free-electron mass or band renormalized mass) and n is the density of carriers (electrons or holes). Figure 2(a) shows that for an ideal metal the dc conductivity $\sigma_0 = ne^2\tau/m$ appears as a local maximum of $\sigma(\omega)$ at zero frequency (Drude peak) and then decays with a Lorentzian form due to finite relaxation time τ . In contrast, $\sigma(\omega) = 0$ for $0 \leq \omega \leq E_g$ in insulators with an optical gap E_g . This Drude definition would categorize some doped FEs with very modest room-temperature conductivity as fundamentally closer to insulators, providing some clarity. In addition, the

nature of the optical conductivity may vary with temperature [51], allowing the metal-insulator classification to change with temperature, thereby accounting for metal-insulator transitions. However, sufficient doping of a ferroelectric can still lead to optical conductivities that remain nonzero as $\omega \rightarrow 0$, but do not reach a local maximum at $\omega = 0$ [Fig. 2(b)], which presents a somewhat ambiguous case.

For first-principles comparisons of metals and insulators, the nonadiabatic Born effective charge (naBEC) is another useful low-frequency dynamical property [52]. Whereas Born effective charges are typically only well defined in insulators (as measurements of the changes in dielectric polarization as a function of atomic displacement), naBECs are made relevant in metals by considering the current generated in response to atomic motion. Atomic motion in this case is produced optically in a regime such that ω is much greater than the inverse carrier lifetime ($1/\tau$) while still being much smaller than interband resonances. If one considers a fictitious limit where $\tau \rightarrow \infty$ and $\omega \rightarrow 0$, the naBECs stabilize as the “Drude weight” or the density of free charge carriers available for conduction. As with optical conductivity, $\omega \rightarrow 0$ in insulators but reaches a nonzero value in metals. The naBECs, as an analog to BECs, are also advantageous as they allow for characterization of polarizability in metals despite polarization itself not being well defined.

Order of magnitude. Although for low frequencies the optical properties of (doped) semiconductors are qualitatively similar ($\sigma \neq 0$), they are quantitatively different because of the difference in carrier masses and densities. At high frequencies, semiconductors and metals both absorb, as expected for an insulator with available conduction band states, owing to interband processes that give rise to finite $\sigma(\omega)$. The frequency crossover at which the behaviors change is given by the plasma frequency ω_p , corresponding to a zero in the real part of the dielectric function. Neglecting any damping effects, the plasma frequency can be expressed as $\omega_p^2 = ne^2/\epsilon\epsilon_0m$, where $\epsilon = \epsilon_\infty$ for a metal in that it includes only electronic contributions from (high-energy) interband transitions while an insulator includes both electronic and ionic (static) polarization contributions, i.e., $\epsilon = \epsilon_\infty + \epsilon_{\text{ionic}}$ and $\epsilon_{\text{ionic}} > \epsilon_\infty$. As the carrier density increases, the plasma frequency increases. In conventional metals, ω_p is in the UV region which gives rise to the UV reflectivity edge (light of frequency $\omega < \omega_p$ is reflected). (In practice, this edge can be difficult to assess experimentally due to interband transitions and in some cases can be found just below visible frequencies.) By contrast, the carrier density in doped semiconductors places ω_p in the 100s of meV (5–30 μm range) as in *n*-InSb (Table I) and is highly tunable [53].

Table I also illustrates the order of magnitude gap in resistivity between doped semiconductors and band metals (as does Fig. 3). The order of magnitude is a meaningful descriptor to aid classification as it similarly is useful for materials selection when deploying materials under application constraints. This distinction should be used when comparing polar metals and doped FEs. However, it is worth noting that some materials would be mislabeled if one uses the order of magnitude of the plasma frequency or resistivity alone. Doped SrTiO₃ exhibits extremely low resistivity (including a

TABLE I. Plasma frequency and resistivity magnitudes as measured at room temperature for band metals (top) and doped semiconductors (bottom).

Material	ω_p (cm ⁻¹)	Resistivity (10 ⁻⁶ Ω m)
Al	1.19×10^5	2.82×10^{-2}
Cu	6.38×10^4	1.70×10^{-2}
Au	7.25×10^4	2.44×10^{-2}
Pb	6.20×10^4	2.20×10^{-1}
Ag	7.25×10^4	1.59×10^{-2}
<i>n</i> -GaAs	4.94×10^2	$\sim 10^3$
<i>n</i> -Si	1.76×10^3	10.7
<i>p</i> -Si	2.28×10^3	6.4
<i>n</i> -InSb	$\sim 2.1 \times 10^2$	10^3 – 10^4

superconducting transition) but the plasma frequency, even at low temperature, is comparable to other doped semiconductors ($\sim 1.5 \times 10^3$ cm⁻¹) [54]. Meanwhile, many polar metals exhibit relatively poor conductivity (Fig. 3), belonging to the so-called class of “bad metals.” LiOsO₃, for example, has a room-temperature resistivity of 15×10^{-6} Ω m and a plasma frequency on the order of $\sim 10^2$ cm⁻¹ [7,55]. Therefore, as with all other descriptors discussed thus far, order of magnitude is best used in combination with other criteria when assessing conductivity.

Doping sensitivity analysis. Although the descriptors above are generally sufficient to clearly differentiate between polar metals and doped FEs, greater clarity may be achieved by

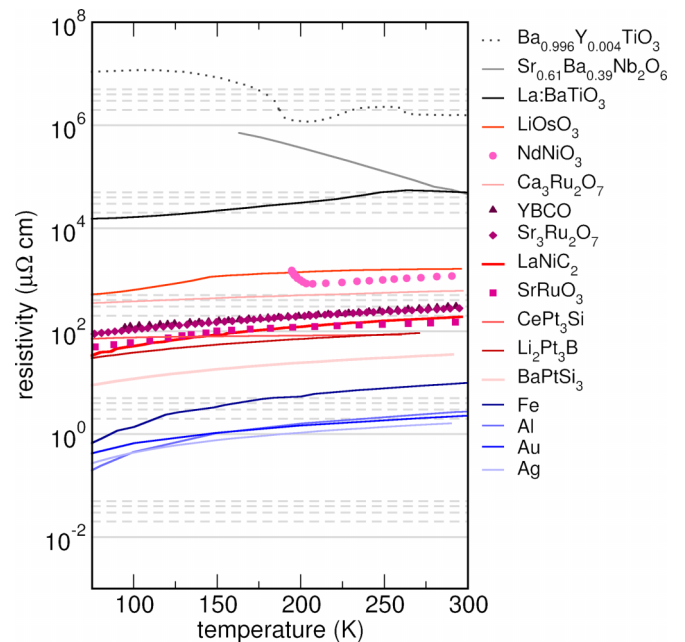


FIG. 3. Temperature-dependent resistivities of a variety of metals, polar metals, and doped semiconductors. Although the polar metals exhibit electron transport roughly one to two orders of magnitude more resistive than typical elemental metals, they are still easily identifiable as significantly more conductive than the doped semiconductors (despite a positive slope in resistivity for La:BaTiO₃ throughout the temperature range).

considering doping as a perturbation to the initial state of a material and evaluating whether that perturbation has been sufficient to change the material's classification. We consider the sensitivity of the electronic and crystallographic structure with respect to the perturbation. The effect of doping on electronic structure is direct and immediately distinguishes intrinsic conductivity from extrinsic conductivity. Doping shifts the Fermi level, which in most metals (i.e., excluding semimetals) has little effect on the effective mass or concentration of the free charge carriers. In a true (multiband) metal, where the Fermi level falls within one or more bands, the electron transport should be effectively unaltered for all but the most extreme changes to the electron chemical potential. This is because the intrinsic carrier density of a metal is high relative to changes induced by the dopants, including changes to scattering and mobility. However, because many of these materials also have other spin and orbital degrees of freedom as discussed later, it is important to understand whether the dopant alters those interactions and not just the carrier density. In some polar metals, the dopant alters the magnetism, which then may produce a metal-insulator transition (even for dilute dopant concentrations). Such scenarios are described later.

In FE insulators, on the other hand, doping has an immediate impact, shifting the Fermi level toward a band edge and often inducing defect states, thereby altering the conduction mechanism. This distinction has practical considerations; the transport properties of doped FEs will be more sensitive to changes in the electron chemical potential than those of polar metals. At sufficiently high concentrations, dopant atoms form a partially occupied impurity band which may exhibit metallic conductivity, so-called degenerately doped semiconductors. In this regime, the conductivity of the material is less sensitive to small variations in the concentration of impurity atoms than a traditional doped semiconductor. However, the system should still be considered a perturbation from the pristine state of the semiconductor and can be distinguished from a band metal by both the relatively smaller carrier concentration and the proximity of the Fermi level within the band gap. These distinctions should be clear from electron transport and optical measurements, respectively.

Predicting the effect of doping on crystal structure is less direct and requires an understanding of the structural driving forces. In the case of polar metals or doped FEs, the primary structural concern is the impact of doping on the inversion-lifting mechanism. Once again, different classes of materials will respond differently to doping as a perturbation. In doped proper FEs, the asymmetric structure is stabilized by a combination of dipole-dipole interactions and covalent bonds which compete with short-range repulsive forces (which favor a higher-symmetry structure) [56–58]. Although the addition of charge carriers is not necessarily incompatible with the persistence of broken symmetry, it cannot help but reduce and eventually eliminate the influence of long-range dipole-dipole interactions (due to the reduction of the screening length) that cooperatively align the off-centering displacements and may also interfere with bonding, depending on the electronic structure of the material. By contrast, long-range interactions in polar metals are always screened and the atoms providing states at the Fermi level typically display weak coupling with the atoms active in the soft phonon(s) driving the symmetry

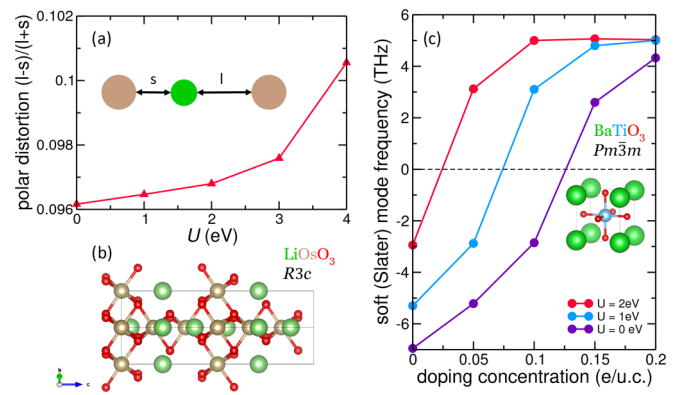


FIG. 4. (a) Adding correlation to LiOsO_3 via increasing the Hubbard U (applied to Os d states) enhances the amplitude of the polar distortion. (Inset) Schematic showing how the polar distortion amplitude is defined by the relative long (ℓ) and short (s) distances between Li and Os along the polar axis. (b) Crystal structure of polar ($R3c$) LiOsO_3 . (c) Increasing the degree of correlation in cubic BaTiO_3 (by applying the Hubbard U to the Ti d states) reduces the critical doping concentration to stabilize the soft Γ -point phonon mode of the cubic phase. (Inset) The crystal structure of cubic ($Pm\bar{3}m$) BaTiO_3 .

break [8]. Nonetheless, for sufficient carrier densities local polar displacements can persist. Therefore, beyond how one simulates doping in these materials, as discussed in the Appendix A, it is also imperative to recognize that *how* we understand the manner in which the atomic structure responds to doping relies intimately on whether the experimental probe interrogates local or average structure [59,60]. In any case, changes in the Fermi level of doped proper FEs will almost always eventually affect the ground-state crystal, local and average, structure whereas similar changes in the Fermi level of polar metals are more likely to leave the crystal structure unaltered, independent of the experimental probe volume.

Electron correlation and magnetism. Correlation also plays a significant role, both in the realization of polar metals generally and in the potential to drive metal-insulator transitions, often in concert with magnetic ordering. Evidence of the former is found in the number of polar metals which exhibit “bad” metallic transport from electron-electron interactions (Fig. 3). Although it is now well established that short-range interactions play a dominant role in driving local off-centering in polar metals, reduction of the screening length via correlation may enable longer-range interactions to further enhance the displacement magnitude, or at least allow for long-range coordination of local displacements. It was shown in Ref. [61] that the polar displacements in the predicted polar metal $\text{SrEuMo}_2\text{O}_6$ are enhanced by introduction of additional correlation via a Hubbard U interaction within density functional theory (DFT). A similar effect is observed when plotting the effective polar amplitude in LiOsO_3 as a function of the static U [Fig. 4(a)]. However, just as correlation may help to stabilize or enhance polar displacements, when coupled with magnetic ordering it may also drive Mott-type metal-insulator transitions, as found in simulations of LiOsO_3 and LiNbO_3 superlattices [62].

The effect of correlation on a system is also highly dependent on the distortion mechanism. In the absence of

magnetism, correlation was shown to reduce the critical free-carrier concentration in doped BaTiO₃ [Fig. 4(c)]. The more highly correlated Ti *d* states exhibited weaker covalent bonding with the O *p* states, favoring the high-symmetry structure. Previous studies of correlation in polar metals implied that correlation should assist in decoupling free charges from the symmetry-lowering transition, but the result of BaTiO₃ illustrates that the impact of correlation is highly dependent on the driving force behind the local off centering.

B. “Ferroelectric” metals

In this section, we consider existing terminology used to denote polar structures in metallic compounds. Most of these labels were developed to describe insulating polar materials and require reevaluation in a metallic context. We discuss the fundamental contradiction inherent to some labels and highlight others which transfer more easily. Note that we are restricting our discussion to polar metals, rather than noncentrosymmetric metals more broadly. Noncentrosymmetric space groups may be polar (more than one point invariant under all symmetry operations), chiral (symmetry elements contain only proper rotations), polar chiral, or nonpolar achiral. Chiral metals in particular (e.g., ferromagnetic MnSi and other B20 transition metal compounds) are of great interest for realizing skyrmions and other emergent physics [63–65], but are not explicitly considered herein. A recent perspective on chiral magnets can be found in Ref. [66], and they are discussed further in the Outlook section.

Contraindicated properties. Whereas long-range coordinated off centering and metallic conductivity were merely thought to be fundamentally incompatible (only to be shown otherwise in the last decade), the switchable polarization of a ferroelectric is, in principle, incapable of coexisting with free charge carriers. A ferroelectric phase is defined as “one in which the spontaneous electric polarization can be reoriented between possible equilibrium directions (determined by the crystallography of the system) by a realizable, appropriately oriented electric field” [67]. Unlike some of the conductivity definitions above, ferroelectricity is an engineering definition; whether a material is ferroelectric can only be confirmed via experimental verification of two criteria: (1) that the polar order occurs at zero electric field (i.e., *spontaneous* ordering) and (2) the polarization may be *switched* via external electric field according to the symmetry of the crystal structure. These two criteria lead to the appearance of domain microstructures, a well-known feature of ferroic properties which separates ferroelectrics from other noncentrosymmetric materials [68]. Gauss’s law prevents the generation of an internal electric field in a metal, thereby screening any attempt to switch the polarization of a polar metal via external electric field and rendering the possibility of criterion (2) null for any reasonably conducting materials.

“*Ferroelectriclike.*” Nevertheless, “ferroelectriclike” or “ferroelectric” (in quotes) terminology has been used to describe structural phase transitions in polar metals since the first report of its kind in 2013 [7], with many other studies since following suit with this naming convention, either in reference to the material itself or to the inversion-lifting transition (e.g., [21,31,41,69]). Despite the recent history of this convention,

describing something as “ferroelectriclike” is inherently ambiguous, as it leaves unclear which aspect(s) of ferroelectricity are being replicated. The comparison to FEs implies that the polarization is switchable, which, as noted above, is only true in very specific cases. The intended FE attribute being referred to is the presence of a second-order, structural phase transition that removes the spatial parity operation of inversion. Given the possibility for confusion, we recommend using more precise terminology.

Ferroelectric bananas. Electrical hysteresis measurements assess the change in charge Q on a pair of electrodes in contact with a dielectric material upon reversal of the applied bias, such that

$$Q = 2P_r A + \sigma E A t, \quad (2)$$

where P_r , A , t , and E are the remnant electric polarization, area of the electrode contact, thickness of the dielectric, and the applied field, respectively, and σ is the conductivity. For either a degenerately doped ferroelectric or a polar metal, $\sigma \neq 0$ and thus the charge that switches is not due to an electric polarization but the finite conductivity of the material, which is well understood to be dielectric loss as $P_r \rightarrow 0$ [36]. Nonetheless, some reports from the literature have claimed both to have synthesized a polar metal and to have measured a polarization [30,70]. However, we find these hysteresis loops reported in Ref. [30] to be consistent with examples from Ref. [36], demonstrating that even definitively nonpolarizable materials (e.g., bananas) can still exhibit electrical hysteresis. Indeed, the classification of a material as a metal is fundamentally incompatible with a bulk polarization within the adiabatic regime [44]. For these reasons, in principle one should not on the one hand call a material a polar metal and then on the other hand report an electric polarization for it.

It is still possible, nonetheless, to experimentally quantify the displacements in polar metals. To this purpose, appropriate techniques such as scanning transmission electron microscopy, near-edge x-ray absorption fine structure, x-ray diffraction, coherent Bragg rod analysis, Raman scattering, and second harmonic generation measurements could be used [16,32,71–74]. The optical conductivity of noncentrosymmetric metals has been used to evaluate the effect and magnitude of correlation effects [16,55]. Analysis of the spectral weights produced in those measurements could be used to derive non-adiabatic Born effective charges (naBECs) and provide insight into the role of various ions with regard to the inversion-breaking mechanism [52].

Ferroelasticity. A ferroelastic material exhibits two or more domains exhibiting a spontaneous strain, the direction of which may be switched by an applied external stress [67,75]. It is the mechanical analog of ferroelectricity. While ferroelectric and ferroelastic transitions are often accompanied by one another (as is the case in BaTiO₃), they may also occur independently since all that is required for a ferroelastic transition is a change in unit cell shape, which may occur either with or without loss of inversion symmetry (e.g., sodium trihydrogen selenite [76] and lithium niobate [77,78] both exhibit nonferroelastic ferroelectric phase transitions). Since ferroelasticity is defined without regard to electric fields or charge carriers, there is no fundamental incompatibility between metallicity and ferroelasticity; therefore, ferroelastic

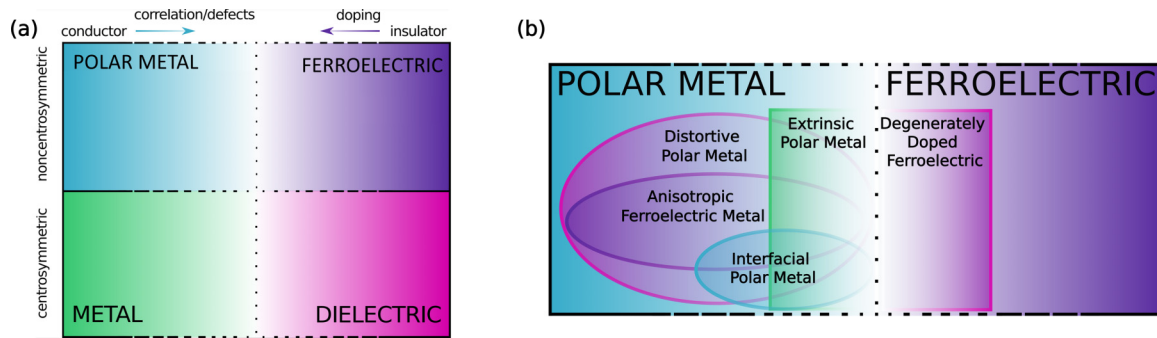


FIG. 5. (a) Using crystal symmetry and electron transport as descriptors, the relationship between polar metals, ferroelectrics, metals, and dielectrics is illustrated. The gradient along the conductivity axis (abscissa) is meant to indicate that the line between metals and insulators is somewhat ambiguous in experiment, whereas the solid colors along the crystal symmetry axis (ordinate) indicate that the presence or lack of an inversion center is precisely defined. (b) A more detailed classification portraying the relationship between the various subclasses defined in the text. Transparency of overlapping categories indicates that a material may belong to multiple subclasses.

metals are a well-defined materials class. However, since they do not necessarily break inversion, we henceforth restrict our discussion of ferroelastic metals to the scenario where the ferroelastic order is coupled with polar displacements.

Switchable polar metals. Recently, a number of materials have emerged which use low dimensionality, anisotropy, or ferroelasticity to demonstrate switchable polar metals [16,18,33]. Although it is still difficult to formally define a polarization ($P \neq 0$) for these compounds, it is possible to reverse the direction of the atomic displacements into an opposite orientation. Perhaps the most widely applicable switching mechanism is ferroelasticity. Although free charges screen external electric fields, strain fields experience no such screening. Although not all polar metals exhibit ferroelastic domains, a change in lattice parameters often accompanies polar distortions, making ferroelastic switching perhaps a viable switching strategy as demonstrated by Lei *et al.* [16].

Switching the polar displacement via electric fields was only achieved recently within two-dimensional polar metals that exhibit anisotropic conductivity [18,33]. With the polar axis oriented perpendicular to the plane, the minimal thickness of the conducting layer limits the number of free charges available to screen an applied electric field. This approach skirts the fundamental conundrum between metallicity and switchable polarization by compromising the conductivity of the polar metal along the polar axis, such that switching is enabled along the more insulating direction. We might argue that the ferroelectric properties associated with these compounds are not intrinsic to the materials themselves but rather a product of the architecture and dimensionality of their synthesis.

We should note that although it has yet to be realized in experiment, there is a third proposed mechanism toward switching a polar metal. Namely, a thin polar metal film is deposited on a FE with low lattice mismatch. An external electric field switches the FE substrate and the resulting strain switches the polar metal [31,79]. This approach might be considered a variation of the ferroelastic switching mechanism, as both approaches use the unscreened strain field to switch polarization.

Piezoelectric metals. Piezoelectricity is defined as a change in polarization in response to a mechanical stress, the only

prerequisite for which is a lack of an inversion center in a dielectric. The cubic enantiomorphic group 432 is the only noncentrosymmetric class that is not piezoactive. However, as was observed when discussing “ferroelectric” metals, polarization in a metal is ill defined. Nonetheless, the Berry curvature effects observed in noncentrosymmetric insulators give rise to analogous properties in metals. Although a static polarization has no meaning in a conductive material, changes in electric polarization are instead measurable as a bulk current, making piezoelectric metals a meaningful designation. Varjas *et al.* also demonstrated that noncentrosymmetric metals with broken time-reversal symmetry should exhibit a magnetopiezoelectric effect (MPE) [9], as was observed recently in antiferromagnetic EuMnBi_2 [80]. It is noteworthy that while all ferroelectrics by definition must exhibit piezoelectricity, not all piezoelectrics will be ferroelectric. This distinction is especially significant in metallic systems as the vast majority of polar metallic systems are not switchable, making “piezoelectric metal” a more accurate and more frequently applicable label than “ferroelectric metal”.

III. CLASSIFYING METALLIC AND POLAR MATERIALS

A. New terminology

Summarizing the above considerations and descriptors concerning symmetry and conductivity class [Fig. 5(a)], we have identified four unique subclasses of polar metals (Table II), which we describe in detail next and differentiate from degenerately doped ferroelectrics. In some cases, a material may be classified by more than one designation as indicated by the overlapping intersections in Fig. 5(b). We then use this schema to survey known metallic and acentric compounds in the literature (Table III), which is current as of December 2022. Figure 6 shows the distribution of these compounds by polar metal subclass and crystal class. A dynamic version of Table III is maintained at [81]. We invite researchers to submit entries as new materials are discovered by contacting the corresponding author.

Polar metal. A polar metal (PM) exhibits a polar crystal structure, identifiable via structural characterization techniques, such as x-ray diffraction, neutron diffraction, or the observation of properties associated with broken inversion

TABLE II. Minimal requirements for various classes of polar metals (PM) by subclass according to the number of phases, crystallography, electrical conductivity, and sensitivity to boundary conditions, e.g., geometry and doping. The two-phase designation is inclusive of hetero-junctions and related nanoscale composite materials. Polar atomic structures in single-phase compounds should adopt one of the 10 polar crystal classes: 1, 2, 3, 4, 6, m , $mm2$, $3m$, $4mm$, $6mm$. Check marks (\checkmark) and crosses (\times) indicate strict positive or negative requirements for that class, respectively, whereas a center dot (\cdot) indicates the presence or absence of the feature does not determine the class assignment for the material.

Phases	Class/Subclass	Polar atomic structure	Local maximum $\sigma(\omega)$	Phase transition	Conduction		Switchable polarization	Doping sensitive
					3D	2D		
1	Polar metal	\checkmark	\checkmark	\cdot	\cdot	\checkmark	\cdot	\times
1	Distortive (DPM)	\checkmark	\checkmark	\checkmark	\cdot	\checkmark	\cdot	\times
1	Anisotropic (AFM)	\checkmark	\checkmark	\cdot	\times	\checkmark	\checkmark	\times
1	Extrinsic (EPM)	\checkmark	\checkmark	\cdot	\cdot	\checkmark	\cdot	\times
2	Interfacial (IPM)	\checkmark	\checkmark	\cdot	\cdot	\checkmark	\cdot	\times
1,2	Degenerately doped ferroelectric (DDF)	\checkmark	\cdot	\cdot	\cdot	\checkmark	\cdot	\checkmark

symmetry (i.e., second harmonic generation). A polar metal should also conduct electricity, as determined via a local maximum in its optical conductivity as $\omega \rightarrow 0$. Finally, the inversion-lifting mechanism and electron transport should be more or less unaffected by small changes in electron concentration, i.e., perturbations to the electron chemical potential. Restated, for a material to be considered a polar metal, the polar distortion and metallicity should not be contraindicated. Examples include LiOsO_3 [7], $\text{Ca}_3\text{Ru}_2\text{O}_7$ [16,17], and CePt_3Si [82].

Distortive polar metal. A distortive polar metal (DPM) is a subclass of polar metals, meeting all of the above criteria while also exhibiting an inversion-symmetry-lifting phase transition from a centrosymmetric to polar crystal class. This eliminates the need for misleading ferroelectriclike terminology and its derivatives by highlighting the intended comparison to a ferroelectric phase transition and not a polarization-field hysteresis measurement.

The distortive polar metal subclass also separates polar metals exhibiting phase transitions from polar metals in which inversion is lifted via compositional order and nominally absent for a broad temperature range. This is a meaningful distinction, both from a fundamental physics perspective as well as an application-driven perspective, as the presence of a phase transition implies opportunities to tune physical properties in ways that would not be possible in polar metals that do not undergo a phase transition. Structural phase transitions in polar metals have been experimentally observed via second-order changes in electronic transport, heat capacity, magnetic susceptibility, dielectric response, second harmonic generation, and with scattering and diffraction techniques [7,41,49,73,83–85]. Within distortive polar metals, as is true with ferroelectrics, the phase transition may be displacive, order-disorder, or exhibit characteristics of both. Examples of distortive polar metals include LiOsO_3 (primarily order-disorder) [7,32,73,74] and $\text{Pb}_2\text{CoOsO}_6$ (primarily displacive) [83]. Examples of nondistortive or compositional polar metals include intermetallics such as CePt_3Si [82] and ErPdBi [86].

In differentiating between polar metals that exhibit a structural phase transition and those that do not, a key feature

of potential technological use in distortive polar metals is their domain structure. Metallic domain walls in ferroelectrics like BiFeO_3 [87] and YMnO_3 [88] are actively investigated for use as nondestructive resistance-based memory devices [89,90]. Similarly, in $\text{Ca}_3\text{Ru}_2\text{O}_7$, both charged and uncharged domain walls were shown to exist, each exhibiting different electrical conductivity, implying potential application in charge-mediated memory devices as well [71]. However, under the current classification scheme, $\text{Ca}_3\text{Ru}_2\text{O}_7$ would not be classified as a distortive polar metal because the temperature at which it would undergo a structural phase transition to recover centrosymmetry exceeds the melting temperature of the compound.

A number of polar metals both exhibit a local ordering mechanism and fail to exhibit an inversion-lifting structural phase transition. $\text{Ca}_3\text{Ru}_2\text{O}_7$ is one such example, in which the polar order is derived from trilinear coupling between octahedral rotations and a polar mode but the thermal energy required to overcome this coupling and achieve a centrosymmetric structure is greater than the melting temperature of the compound [16,17]. Therefore, materials which exhibit local-ordering mechanisms similar to those observed in distortive polar metals may be called “pseudodistortive polar metals.” This terminology acknowledges that such materials share important characteristics with distortive metals while remaining distinct due to their lack of an ordering transition.

Anisotropic ferroelectric metal. An anisotropic ferroelectric metal (AFM) meets the structural criteria for a distortive polar metal but exhibits limited conductivity along the polar axis, allowing for observable switching of the polar displacement direction via an external electric field. “Anisotropic” is meant to call attention to the fact that the largest conductivity tensor element and direction of the polar distortions are in transverse orientations. As a consequence, these materials can be deployed in suitable device geometries to sidestep the fundamentally contraindicated relationship between field-switchable polarization and conductivity. Ferroelectricity is not, and by definition cannot be, an intrinsic property of a metal, but low-dimensional conductors provide a design strategy to achieve high electrical anisotropy such that the

TABLE III. Published polar compounds exhibiting metallic conductivity. Columns denote space group (SG), presence of a polar structural phase transition (T_c), presence of a superconducting transition (T_{sc}), and presence of a magnetic ordering transition (T_M), respectively. Under SG: * = only the point group is known; “unknown” = the specific symmetry elements are unknown but there is evidence of broken inversion symmetry. Under T_c : P = compound is predicted but has not yet been synthesized. Under Class, the following abbreviations are used: polar metal (PM), distortive polar metal (DPM), anisotropic ferroelectric metal (AFM), extrinsic polar metal (EPM), interfacial polar metal (IPM), and degenerately doped ferroelectric (DDF).

Composition	SG	T_c	T_{sc}	T_M	Class	Digital object identifier (DOI)
BaTiO ₃	<i>P4mm</i>	yes			DDF	10.1038/s41598-017-04635-3
BaTiO _{3-δ}	<i>P4mm</i>	yes			DDF	10.1103/PhysRevLett.104.147602
PbTiO _{3-δ}	<i>P4mm</i>	P			EPM	10.1103/PhysRevB.94.224107
PbTi _{1-x} Nb _x O ₃	<i>P4mm</i>				EPM	10.1103/PhysRevB.96.165206
BiFeO _{3-δ}	<i>R3c</i>	P		yes	EPM	10.1103/PhysRevB.93.174110
Sr _{1-x} Ca _x TiO _{3-δ}	<i>P4mm</i>	yes	yes		DPM	10.1038/NPHYS4085
BaMnO ₃	<i>Amm2</i>	P			EPM	10.1103/PhysRevB.97.054107
BiAlO ₃	<i>P4mm</i>	P			EPM	10.1103/PhysRevB.97.054107
BaTiO ₃ /SrTiO ₃ /LaTiO ₃	<i>mm4*</i>				IPM	10.1038/s41467-018-03964-9
LaAlO ₃ /BaSr _{0.8} TiO ₃ /SrTiO ₃	unknown				IPM	10.1038/s42005-019-0227-4
LaFeO ₃ /YFeO ₃	<i>Pmc2₁</i>	P			IPM	10.1103/PhysRevB.97.054107
NdNiO ₃	<i>Pc</i>				PM	10.1038/nature17628
LaNiO ₃	<i>Pc</i>				PM	10.1038/nature17628
LiOsO ₃	<i>R3c</i>	yes			DPM	10.1038/NMAT3754
LiNbO ₃	<i>R3c</i>	P			DDF	10.1103/PhysRevMaterials.3.054405
MgReO ₃	<i>R3c</i>	P			PM	10.1103/PhysRevB.90.094108
TiGaO ₃	<i>R3c</i>	P			PM	10.1103/PhysRevB.90.094108
Ca ₃ Ru ₂ O ₇	<i>Bb2_{1m}</i>			yes	PM	10.1021/acs.nanolett.8b00633
(Sr,Ca)Ru ₂ O ₆	<i>Pmc2₁</i>	P		yes	PM	10.1088/0953-8984/26/26/265501
Bi ₅ Ti ₅ O ₁₇	<i>Pm2_{1n}</i>	P			AFM	10.1038/ncomms11211
BiPbTi ₂ O ₆	<i>Pmm2</i>	P			PM	10.1038/s43246-019-0005-6
La ₂ Ti ₂ O ₇	<i>P2₁</i>	P			EPM	10.1103/PhysRevB.97.054107
Sr ₂ Nb ₂ O ₇	<i>Cmc2₁</i>	P			EPM	10.1103/PhysRevB.97.054107
MgCNi ₃	<i>P4mm</i>	P			PM	10.1103/PhysRevMaterials.2.125004
ZnCNi ₃	<i>P4mm</i>	P			PM	10.1103/PhysRevMaterials.2.125004
CdCNi ₃	<i>P4mm</i>	P			PM	10.1103/PhysRevMaterials.2.125004
CeSiPt ₃	<i>P4mm</i>		yes	yes	PM	10.1103/PhysRevLett.92.027003
LiGaGe	<i>P6_{3mc}</i>				PM	10.1103/PhysRevB.99.195154
SrHgPb	<i>P6_{3mc}</i>	P			PM	10.1103/PhysRevLett.121.106404
SrHgSn	<i>P6_{3mc}</i>	P			PM	10.1103/PhysRevLett.121.106404
CaHgSn	<i>P6_{3mc}</i>	P			PM	10.1103/PhysRevLett.121.106404
KMgSb _{0.2} Bi _{0.8}	<i>P6_{3mc}</i>	P			PM	10.1103/PhysRevLett.117.076401
CaAgBi	<i>P6_{3mc}</i>	P			PM	10.1103/PhysRevMaterials.1.044201
LiZnBi	<i>P6_{3mc}</i>	P			PM	10.1103/PhysRevB.96.115203
LaAuGe	<i>P6_{3mc}</i>				PM	10.1063/1.5132339
LaPtSb	<i>P6_{3mc}</i>				PM	10.1063/1.5132339
WTe ₂	<i>Pnm2₁</i>	yes	yes		AFM	10.1038/s41586-018-0336-3
MoTe ₂	<i>Pnm2₁</i>	yes			PM	10.1126/sciadv.1601378
CrN	<i>6mm*</i>			yes	AFM	10.1103/PhysRevB.96.235415
CrB ₂	<i>6mm*</i>	P		yes	AFM	10.1103/PhysRevB.96.235415
FeB ₂	<i>6mm*</i>				AFM	10.1021/acs.nanolett.6b02335
P	<i>P6_{3mc}</i>	P			PM	10.1088/1361-648X/aadeaa
As	<i>P6_{3mc}</i>	P			PM	10.1088/1361-648X/aadeaa
Sb	<i>P6_{3mc}</i>	P			PM	10.1088/1361-648X/aadeaa
Bi	<i>P6_{3mc}</i>	P			PM	10.1088/1361-648X/aadeaa
SnP	<i>I4mm</i>	yes	yes		DPM	10.1103/PhysRevLett.119.207001
PdBi	<i>P2₁</i>		yes		PM	10.1016/j.phpro.2013.04.062
UIr	<i>P2₁</i>		yes	yes	PM	10.1007/978-3-642-24624-1_2
LaNiC ₂	<i>Amm2</i>		yes	yes	PM	10.1016/j.physc.2014.01.008
NdRhC ₂	<i>Amm2</i>			yes	PM	10.1021/cm00006a007
PrRhC ₂	<i>Amm2</i>			yes	PM	10.1021/cm00006a007
LaSr ₂ Cu ₂ GaO ₇	<i>Ima2</i>		yes	yes	PM	10.1021/cm00017a032
CeSr ₂ Cu ₂ GaO ₇	<i>Ima2</i>		yes	yes	PM	10.1021/cm00017a032

TABLE III. (Continued.)

Composition	SG	T_c	T_{sc}	T_M	Class	Digital object identifier (DOI)
PrSr ₂ Cu ₂ GaO ₇	<i>Ima2</i>		yes	yes	PM	10.1021/cm00017a032
NdSr ₂ Cu ₂ GaO ₇	<i>Ima2</i>		yes	yes	PM	10.1021/cm00017a032
PmSr ₂ Cu ₂ GaO ₇	<i>Ima2</i>		yes	yes	PM	10.1021/cm00017a032
SmSr ₂ Cu ₂ GaO ₇	<i>Ima2</i>		yes	yes	PM	10.1021/cm00017a032
EuSr ₂ Cu ₂ GaO ₇	<i>Ima2</i>		yes	yes	PM	10.1021/cm00017a032
GdSr ₂ Cu ₂ GaO ₇	<i>Ima2</i>		yes	yes	PM	10.1021/cm00017a032
TbSr ₂ Cu ₂ GaO ₇	<i>Ima2</i>		yes	yes	PM	10.1021/cm00017a032
DySr ₂ Cu ₂ GaO ₇	<i>Ima2</i>		yes	yes	PM	10.1021/cm00017a032
HoSr ₂ Cu ₂ GaO ₇	<i>Ima2</i>		yes	yes	PM	10.1021/cm00017a032
ErSr ₂ Cu ₂ GaO ₇	<i>Ima2</i>		yes	yes	PM	10.1021/cm00017a032
TmSr ₂ Cu ₂ GaO ₇	<i>Ima2</i>		yes	yes	PM	10.1021/cm00017a032
YbSr ₂ Cu ₂ GaO ₇	<i>Ima2</i>		yes	yes	PM	10.1021/cm00017a032
YSr ₂ Cu ₂ GaO ₇	<i>Ima2</i>		yes	yes	PM	10.1021/cm00017a032
V ₂ Hf	<i>Imm2</i>	yes	yes		DPM	10.1103/PhysRevB.17.1136
Li ₂ IrSi ₃	<i>P3₁c</i>		yes		PM	10.7566/JPSJ.83.093706
Mg ₂ Al ₃	<i>R3m</i>	yes	yes		DPM	10.1103/PhysRevB.76.014528
La ₃ B ₂ C ₆	<i>P4</i>		yes		PM	10.1016/0022-5088(83)90520-9
BaPtSi ₃	<i>I4mm</i>		yes		PM	10.1103/PhysRevB.80.064504
CeIrSi ₃	<i>I4mm</i>		yes	yes	PM	10.1143/JPSJS.77SA.37
CeRhSi ₃	<i>I4mm</i>		yes	yes	PM	10.1143/JPSJ.76.051010
LaPtSi ₃	<i>I4mm</i>		yes		PM	10.1103/PhysRevB.89.094509
LaPdSi ₃	<i>I4mm</i>		yes		PM	10.1103/PhysRevB.89.094509
CeIrGe ₃	<i>I4mm</i>		yes	yes	PM	10.1016/j.jmmm.2006.10.151
EuNiGe ₃	<i>I4mm</i>			yes	PM	10.1103/PhysRevB.87.064406
LaRhGe ₃	<i>I4mm</i>				PM	10.1063/5.0042924
IrRhGe ₃	<i>I4mm</i>				PM	10.1063/5.0042924
PdRhGe ₃	<i>I4mm</i>				PM	10.1063/5.0042924
SrPdGe ₃	<i>I4mm</i>		yes		PM	10.1088/1742-6596/273/1/012078
SrPtGe ₃	<i>I4mm</i>		yes		PM	10.1088/1742-6596/273/1/012078
PrPdIn ₂	<i>I4mm</i>			yes	PM	10.1021/cm031139m
CePt ₃ Si	<i>I4mm</i>		yes	yes	PM	10.1103/PhysRevLett.92.027003
Li ₂ (Pd _{1-x} Pt _x) ₃ B	<i>I4mm</i>		yes	yes	PM	10.1088/1742-6596/400/2/022096
KCu ₇ P ₃	<i>P31m</i>				PM	10.1021/acs.inorgchem.9b01336
Bi ₂ FeCrO ₆	<i>R3</i>	P		yes	PM	10.1103/PhysRevLett.123.107201
CeAuGe	<i>P6₃mc</i>			yes	PM	10.1016/0304-8853(95)00430-0
LuAuGe	<i>P6₃mc</i>				PM	10.1016/0925-8388(95)02069-1
ScAuGe	<i>P6₃mc</i>				PM	10.1016/0925-8388(95)02069-1
HoAuGe	<i>P6₃mc</i>			yes	PM	10.1088/0953-8984/13/11/315
CeCuSn	<i>P6₃mc</i>				PM	10.1016/j.jallcom.2004.09.086
La ₁₅ Ge ₉ C	<i>P6₃mc</i>				PM	10.1016/j.jallcom.2011.03.092
La ₁₅ Ge ₉ Fe	<i>P6₃mc</i>			yes	PM	10.1021/ic9515158
La ₁₅ Ge ₉ Co	<i>P6₃mc</i>				PM	10.1021/ic9515158
La ₁₅ Ge ₉ Ni	<i>P6₃mc</i>				PM	10.1021/ic9515158
Sr ₃ Cu ₈ Sn ₄	<i>P6₃mc</i>				PM	10.1016/j.intermet.2011.02.018
IrMg _{2.03} In _{.97}	<i>P6₃mc</i>				PM	10.1016/j.intermet.2003.12.001
IrMg _{2.20} In _{.80}	<i>P6₃mc</i>				PM	10.1016/j.intermet.2003.12.001
CaAlSi	<i>P6₃</i>		yes		PM	10.1143/JPSJ.75.043713
TlV ₆ S ₈	<i>P6₃</i>		yes		PM	10.1016/S0038-1098(01)00333-7
KV ₆ S ₈	<i>P6₃</i>		yes		PM	10.1016/S0038-1098(01)00333-7
RbV ₆ S ₈	<i>P6₃</i>		yes		PM	10.1016/S0038-1098(01)00333-7
CsV ₆ S ₈	<i>P6₃</i>		yes		PM	10.1016/S0038-1098(01)00333-7
LaPt ₃ B	<i>P4mm</i>			yes	PM	10.1016/S0925-8388(03)00373-6
PrPt ₃ B	<i>P4mm</i>			yes	PM	10.1016/S0925-8388(03)00373-6
NdPt ₃ B	<i>P4mm</i>			yes	PM	10.1016/S0925-8388(03)00373-6
LaRhSi ₃	<i>I4mm</i>		yes		PM	10.1016/0025-5408(84)90017-5
LaIrSi ₃	<i>I4mm</i>		yes		PM	10.1016/0025-5408(84)90017-5
CeCoGe ₃	<i>I4mm</i>		yes	yes	PM	10.1016/j.jmmm.2006.10.717
LaCoGe ₃	<i>I4mm</i>			yes	PM	10.1143/JPSJ.75.044711
CeRhGe ₃	<i>I4mm</i>		yes	yes	PM	10.1143/JPSJ.77.064716

TABLE III. (Continued.)

Composition	SG	T_c	T_{sc}	T_M	Class	Digital object identifier (DOI)
CeRuSi ₃	<i>I4mm</i>				PM	10.1143/JPSJ.77.064716
LaIrGe ₃	<i>I4mm</i>				PM	10.1143/JPSJ.77.064717
LaFeGe ₃	<i>I4mm</i>				PM	10.1143/JPSJ.77.064717
PrCoGe ₃	<i>I4mm</i>				PM	10.1143/JPSJ.77.064717
CaIrSi ₃	<i>I4mm</i>		yes		PM	10.1016/j.physc.2009.10.120
CaPtSi ₃	<i>I4mm</i>		yes		PM	10.1134/S0021364010170157
SrAuSi ₃	<i>I4mm</i>		yes		PM	10.1021/cm500032u
EuPdGe ₃	<i>I4mm</i>			yes	PM	10.1016/j.ssc.2012.02.022
EuPtSi ₃	<i>I4mm</i>			yes	PM	10.1103/PhysRevB.81.144414
NdPdIn ₂	<i>I4mm</i>				PM	10.1021/cm031139m
SmPdIn ₂	<i>I4mm</i>				PM	10.1021/cm031139m
GdPdIn ₂	<i>I4mm</i>				PM	10.1021/cm031139m
ErPdIn ₂	<i>I4mm</i>				PM	10.1021/cm031139m
TmPdIn ₂	<i>I4mm</i>				PM	10.1021/cm031139m
LuPdIn ₂	<i>I4mm</i>				PM	10.1021/cm031139m
La ₂ NiAl ₇	<i>I4mm</i>				PM	10.1021/cm050513a
SnP	<i>I4mm</i>				PM	10.1021/ic50084a032
GeP	<i>I4mm</i>		yes		PM	10.1016/0022-4596(70)90005-8
Ir ₉ Al ₂₈	<i>P3₁c</i>				PM	10.1016/j.jallcom.2005.06.027
γ -Bi ₂ Pt	<i>P3₁m</i>				PM	10.1002/zaac.201400331
Au _{6.05} Zn _{12.51}	<i>P3₁m</i>				PM	10.1021/ic301933a
Ba ₂₁ Al ₄₀	<i>P3₁m</i>				PM	10.1021/ic0400235
Li ₁₇ Ag ₃ Sn ₆	<i>P3₁m</i>				PM	10.1021/ja038868n
Cr ₅ Al ₈	<i>R3m</i>				PM	10.1107/S0567740874004997
Mn ₅ Al ₈	<i>R3m</i>	yes			DPM	10.1007/BF02672582
Cu _{7.8} Al ₅	<i>R3m</i>				PM	10.1107/S0108768191005694
Cu ₇ Hg ₆	<i>R3m</i>				PM	10.3891/acta.chem.scand.23-1181
NbS ₂	<i>R3m</i>		yes		PM	10.1107/S0567740874003220
Pr ₂ Fe ₁₇	<i>R3m</i>			yes	PM	10.1103/PhysRevB.68.054424
Pr ₂ Co ₁₇	<i>R3m</i>				PM	10.1103/PhysRevB.68.054424
Sn ₄ As ₃	<i>R3m</i>		yes		PM	10.1002/zaac.19683630102
Sn ₄ P ₃	<i>R3m</i>		yes		PM	10.1002/zaac.19683630102
LiOsO ₃	<i>R3c</i>	yes			DPM	10.1038/NMAT3754 A
La ₄ Mg ₅ Ge ₆	<i>Cmc2₁</i>				PM	10.1021/ic2014732
La ₄ Mg ₇ Ge ₆	<i>Cmc2₁</i>				PM	10.1021/ic2014732
Yb ₂ Ga ₄ Ge ₆	<i>Cmc2₁</i>				PM	10.1002/chem.200305755
Ce ₂ Rh ₃ (Pb,Bi) ₅	<i>Cmc2₁</i>			yes	PM	10.1016/j.jssc.2007.06.012
Eu ₂ Pt ₃ Sn ₅	<i>Cmc2₁</i>			yes	PM	10.1524/zkri.2009.1160
Lu ₄ Zn ₅ Ge ₆	<i>Cmc2₁</i>				PM	10.1016/j.intermet.2013.02.018
Hg ₃ Te ₂ Br ₂	<i>R3</i>	yes			PM	10.1038/s41467-021-21836-7
In ₂ S ₃	<i>R3m</i>	P			AFM	10.1039/D1MH01556G
In ₂ Se ₃	<i>R3m</i>	P			AFM	10.1039/D1MH01556G
In ₂ Te ₃	<i>R3m</i>	P			AFM	10.1039/D1MH01556G
NaYMnReO ₃	<i>P2₁</i>	P		yes	PM	10.1021/acs.chemmater.0c02976
NaYFeReO ₃	<i>P2₁</i>	P		yes	PM	10.1021/acs.chemmater.0c02976
NaYCoReO ₃	<i>P2₁</i>	P		yes	PM	10.1021/acs.chemmater.0c02976
NaYNiReO ₃	<i>P2₁</i>	P		yes	PM	10.1021/acs.chemmater.0c02976
NaYMnOsO ₃	<i>P2₁</i>	P		yes	PM	10.1021/acs.chemmater.0c02976
NaYCoOsO ₃	<i>P2₁</i>	P		yes	PM	10.1021/acs.chemmater.0c02976
NaYNiOsO ₃	<i>P2₁</i>	P		yes	PM	10.1021/acs.chemmater.0c02976
NaYFeWO ₃	<i>P2₁</i>	P		yes	PM	10.1021/acs.chemmater.0c02976
YAl ₂	<i>P6mm</i>	P			AFM	10.1021/acs.jpcclett.0c03136
CaRh ₂	<i>P6mm</i>	P			AFM	10.1021/acs.jpcclett.0c03136
doped SiGe	<i>P3m1</i>	P			AFM	10.1088/1361-648X/abdce9/pdf
doped SiSn	<i>P3m1</i>	P			AFM	10.1088/1361-648X/abdce9/pdf
doped GeSn	<i>P3m1</i>	P			AFM	10.1088/1361-648X/abdce9/pdf
KNbO ₃ /BaTiO ₃	<i>P4mm</i>	P		yes	AFM	10.1016/j.commsci.2020.110235
(SrRuO ₃) ₁ /(BaTiO ₃) ₁₀	<i>mm2*</i>			yes	AFM	10.1021/acs.nanolett.0c03417
strained EuTiO _{3-x} H _x	<i>Pmm2</i>	P		yes	EPM	10.1103/PhysRevB.102.224102

TABLE III. (Continued.)

Composition	SG	T_c	T_{sc}	T_M	Class	Digital object identifier (DOI)
KTiO ₂ H	unknown	P	yes		DDF	10.1103/PhysRevMaterials.5.054802
RbTiO ₂ H	unknown	P	yes		DDF	10.1103/PhysRevMaterials.5.054802
CsTiO ₂ H	unknown	P	yes		DDF	10.1103/PhysRevMaterials.5.054802
doped PbZrO ₃	unknown	P			DDF	10.1103/PhysRevB.102.134118
LaFeAsO _{1-x} H _x	<i>mm2*</i>		yes	yes	PM	10.21203/rs.3.rs-77544/v1
Pb ₂ CoOsO ₆	<i>Pc</i>	yes		yes	DPM	10.1103/PhysRevB.102.144418
PrAlGe	<i>I4₁md</i>			yes	PM	10.1038/s41467-020-16879-1
doped PbTe monolayer	<i>P3m1</i>	P			EPM, AFM	10.1039/d0nh00188k
en-CoS	<i>Pca2₁</i>			yes	PM	10.1021/acs.chemmater.1c00540
Eu(Ti _{0.875} Nb _{0.125}) ₃	<i>P4mm</i>	P	yes	E	EPM	10.48550/arXiv.2203.10646
Bi ₅ Mn ₅ O ₁₇	<i>Pmn2₁/Pm2₁n</i>	P	yes	A	AFM	10.1038/s41467-020-18664-6
2D In	<i>3m*</i>				PM	10.1021/acs.nano.1c05944
2D Ga	<i>3m*</i>				PM	10.1021/acs.nano.1c05944
2D In/Ga	<i>3m*</i>				PM	10.1021/acs.nano.1c05944
(Fe _{0.5} Co _{0.5}) ₅ GeTe ₂	<i>P6₃mc</i>			yes	PM	10.1126/sciadv.abm7103
GdCaMnNiO ₆	<i>P2₁</i>	P	yes		PM	10.2139/ssrn.4147202
LaCaMnNiO ₆	<i>P2₁</i>	P	yes		PM	10.2139/ssrn.4147202
SmCaMnNiO ₆	<i>P2₁</i>	P	yes		PM	10.2139/ssrn.4147202
TmCaMnNiO ₆	<i>P2₁</i>	P	yes		PM	10.2139/ssrn.4147202
SrTiO ₃ -based 2DEGs	unknown	Yes	Yes	Yes	IPM, AFM, DPM	10.1002/adma.201200667 10.1103/PhysRevMaterials.4.041002 10.1038/s41586-020-2197-9
Doped GeTe	<i>R3m</i>	Yes	Yes	Yes	DPM, AFM	10.1038/ncomms15033 10.1103/PhysRevLett.112.047202

polarization becomes switchable by external electric field. Examples include WTe₂ [18] and Bi₅Ti₅O₁₇ [33]. Note that polar metals whose polar order is switched via strain are not classified as anisotropic ferroelectric metals, as this switching mechanism does not require limiting the fundamental relationship between an external electric field and free charge carriers.

Extrinsic polar metal. An extrinsic polar metal (EPM) must meet each of the structural and electronic criteria of a polar metal (i.e., polar structure, metallic optical conductivity, robust polar distortion in the presence of perturbations to the Fermi level). However, a polar metal is deemed extrinsic if the metallic electron transport is a result of perturbations to the pristine state of the material. The number of charge carriers or conductivity of an extrinsic polar metal is determined by the doping mechanisms, such as chemical substitution,

interstitials, vacancies, photodoping, and electrostatic gating. This distinction has consequences for application contexts in which sensitivity to small changes in chemical potential either positively or detrimentally impact performance. In any case, the broken inversion symmetry in an extrinsic polar metal persists over the doping ranges explored. Examples include Nb-doped PbTiO₃ [12] and doped SrTiO₃ [13, 14].

Interfacial polar metal. When the two fundamental criteria for a polar metal exist only at the interface between two compounds, we define the resulting composite material as an interfacial polar metal (IPM). Interfacial polar metals exhibit some similarity to both anisotropic ferroelectric metals and extrinsic polar metals, but can be fundamentally distinguished from both. Whereas anisotropic ferroelectric metals often exhibit low-dimensional electronic structures distinct from bulk polar metals, interfacial polar metals emerge out of the heterojunction created by interfacing two materials which in the bulk are either nonmetallic, nonpolar, or both. In this sense, either the conductivity, the broken inversion symmetry, or both should be exclusively limited to the interface. In addition, whereas anisotropic ferroelectric metals must be switchable, interfacial polar metals may or may not be switchable.

When the interfacial polar metal forms at the interface of two extrinsically or self-doped semiconductors, it may be considered a subclass of extrinsic polar metals. However, if no doping is required or if one of the two materials is a bulk conductor, then the conductivity of the interface is no longer considered to be extrinsically derived. The most well-known buried interfacial polar metals belong to the family of SrTiO₃-based two-dimensional electron gases (2DEGs), of which LaAlO₃/SrTiO₃ is perhaps the most well studied [91]. The SrTiO₃-based

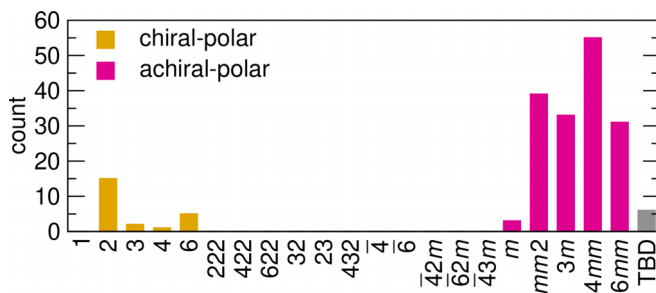


FIG. 6. Distribution of 190 polar metals in Table III among the 21 noncentrosymmetric crystal classes. Most polar metals are found in achiral-polar symmetries rather than chiral-polar symmetries. The symmetry of compounds labeled “TBD” remains to be determined.

2DEGs illustrate the incredible diversity and versatility of interfacial polar metals, capable of hosting a switchable polarization, multiferroic order, and other emerging properties [92–94]. Perovskite superlattices have been used to generate many other well-known interfacial polar metals, including BaTiO₃/SrTiO₃/LaTiO₃ [95], LaAlO₃/BaSr_{0.8}TiO₃/SrTiO₃ [96], and doped LaFeO₃/YFeO₃ [97].

Degenerately doped ferroelectric. A degenerately doped ferroelectric (DDF) meets the same structural criteria as the other categories, but the structural transition is detrimentally impacted by perturbations to the Fermi level from a pristine insulating state. In such a material, the polar order and the conduction mechanism are contraindicated, which both implies a fundamentally different relationship between the polar structure and the conduction mechanism than in the above categories. These differences will affect how degenerately doped ferroelectrics are used in devices, e.g., some are proposed for thermoelectric applications [98–101], whereas the higher carrier density in polar metals would make them less well suited for these energy devices. Furthermore, the pristine undoped material is a good dielectric that exhibits a spontaneous and switchable polarization. Nonetheless, if degenerately doping a ferroelectric is seen as a pathway to accessing the many desirable properties of a polar metal, it should be performed in a context where careful control of the chemical potential is possible and practical. The conductivity threshold required to be deemed “degenerately doped” rather than “metallic” is somewhat ambiguous, but a minimum criteria should be $\sigma \neq 0$ as $\omega \rightarrow 0$. The primary example of a degenerately doped ferroelectric is doped BaTiO₃ [15,49,57].

Noncentrosymmetric nonpolar metals. Whereas all polar metals are necessarily noncentrosymmetric, not all noncentrosymmetric metals exhibit polar order. One category of noncentrosymmetric metals absent from our discussion (and therefore Table II and Fig. 5) are those metals which are both noncentrosymmetric and nonpolar. Such compounds can be obtained in two distinct crystal classes: (1) chiral-nonpolar crystal classes or (2) achiral-nonpolar crystal classes.

How would the minimum requirements given in Table II change for these classes? None of the structures in either class would be polar, thus there is no switchable polarization, and the sensitivity of the polarization to doping is not relevant. With no polar order, the dimensionality of the conductivity should not significantly change. Finally, as in the case of polar metals, phase transitions may or may not occur in noncentrosymmetric nonpolar metals. We would also expect some new materials physics in class (1) and class (2) not necessarily accessible in polar metals. For class (1), chiral metals provide anisotropic superexchange that can produce real-space magnetic spin textures, e.g., skyrmions, as in the case of MnSi [102]. The microstructure of the noncentrosymmetric metals in both classes differs from their polar counterparts, but there is limited work on understanding domain structures and grain boundaries in these materials. This would be an interesting future research direction.

B. Classification caveats

Despite the consideration put into the above classification scheme, there remain materials which prove difficult to

categorize into a single class. The majority of such cases involve materials which undergo significant changes in conductivity or displacive mode dynamics as a result of changes in their environment. In most cases, it is simplest to describe a material as moving between categories as a function of some perturbation. For example, a polar material exhibiting a metal-insulator transition would transition from a polar metal to ferroelectric [62,103,104].

Another unique case is found in materials which exhibit a polar displacement that is *enhanced* as a consequence of doping an initially insulating material, as predicted in Sr₃Sn₂O₇ and various binary metal oxides [105,106]. Strictly speaking, assuming doping occurs at such level so as to pass the Drude criterion for conductivity, it would be tempting to categorize Sr₃Sn₂O₇ as a degenerately doped ferroelectric since the polar distortion is sensitive to changes in the Fermi level and the pristine state is ferroelectric. However, since polar order and conductivity are clearly not fundamentally contraindicated in this compound, it may be better to reclassify it as an extrinsic polar metal. Such a classification would be made easier if the polar mode amplitude asymptotes under doping to a finite value and becomes relatively insensitive to changes in the Fermi level. It is also worth noting that the material has not yet been synthesized and characterized in experiment, and we may discover that the real material behaves differently than anticipated.

Finally, although we referenced 2D polar metals in the anisotropic ferroelectric metals subclass, it should be noted that a low-dimensional polar metal may have applications beyond switchability under external electric field. For example, 2D polar metallic In and Ga thin films exhibit remarkable second harmonic generation due to their unique bonding environment and fine control of the crystal lattice [107,108]. These materials cannot be described as ferroelectrics, and would be considered simply polar metals under our current scheme, although the strong coupling between the thin-film morphology and crystal structure implies a similarity to interfacial polar metals and may warrant a separate category entirely.

IV. OUTLOOK

The outlook for polar metals research has never held more possibility. The number of publications in the research space continues to climb and we have made great strides in determining the necessary relationship between electronic and crystallographic structure to enable their coexistence. Although there remain some unanswered questions (e.g., is “weak coupling” a necessary condition or merely a useful design principle?), there are also opportunities to significantly broaden the polar metallic design space:

(i) Polar metals requiring new subclass designations may combine multiple orders or enhanced functions, e.g., magnetism and strong electron-electron interactions can enable magnetochiral anisotropy with nonreciprocal electrical transport.

(ii) Polar metals violating the weak-coupling principle would broaden the materials landscape and bring control routes to physical properties using nonconjugate fields.

Beginning with magnetic polar metals, there are many known acentric conductors with magnetic ordering tem-

peratures (across all of the above categories), including the following: en-CoS [19], $\text{Pb}_2\text{CoOsO}_6$ [83], $\text{Pb}_2\text{NiOsO}_6$ [109], tricolor superlattices $\text{BaTiO}_3/\text{SrTiO}_3/\text{LaTiO}_3$ [95], $\text{Ca}_3\text{Ru}_2\text{O}_7$ [17], and more. In general, the coexistence of any magnetic order with the necessary characteristics of a polar metal described above should be considered the minimal definition of a multiferroic polar metal. These may be further subcategorized based on the type of magnetic order, i.e., ferromagnetic, antiferromagnetic, or helical. Multiferroic polar metals with a switchable polar distortion would constitute an additional subclass, namely, magnetoelectric multiferroic polar metals.

However, the relationship between magnetic ordering in these materials and their designation as polar metals varies. For example, Jiao *et al.* describe separating polar metals with magnetic ordering temperatures into type-I and type-II categories depending on the strength of the coupling between magnetic and polar orders, with $\text{Pb}_2\text{CoOsO}_6$ being an example of a type-II magnetic polar metal [83]. By contrast, the magnetic ordering predicted in $\text{SrCaRu}_2\text{O}_6$ is not expected to couple to the inversion-lifting distortion [8], or one might note the insensitivity of the polar transition in doped SrTiO_3 to the presence of magnetic doping and isovalent substitution as an example of type-I behavior [110]. Still, we may describe other categories, including magnetically driven metal-insulator transitions in $\text{Pb}_2\text{CaOsO}_6$ [111] and B-site substituted $\text{Ca}_3\text{Ru}_2\text{O}_7$ [112–114] (in which case the magnetic and transport properties are highly sensitive to dilute dopant concentrations and dependent on the substituting species, Mn, Ti, or Fe, which alters the magnetic state). Note that indirect perturbation of electronic transport via magnetic interactions does not constitute a violation of the polar metal criterion that electron transport be insensitive to changes in the electron chemical potential. In the case of $\text{Ca}_3\text{Ru}_2\text{O}_7$, if the original AFM-b magnetic ordering is preserved, $\text{Ca}_3\text{Ru}_2\text{O}_7$ will retain both a polar structure and metallic transport independent of doping, as can be easily seen from its electronic band structure [115]. Therefore, $\text{Ca}_3\text{Ru}_2\text{O}_7$ is classified as a polar metal. Depending on the dopant and level of doping, $\text{Ca}_3\text{Ru}_2\text{O}_7$ undergoes an isostructural metal-to-insulator transition. This is due to the alteration of the delicate balance between ferromagnetic and antiferromagnetic exchange interactions [116]. Indeed, while undoped $\text{Ca}_3\text{Ru}_2\text{O}_7$ exhibits a quasi-two-dimensional metallic state with AFM-b magnetic ordering, Ti and Fe doping result in a Mott-insulating state with G-type AFM order and a localized state with coexisting incommensurate and AFM-b magnetic ordering, respectively, as reported in Refs. [113,117]. Subcategorization according to magnetic properties helps describe fundamentally different physical phenomena, but may be well suited to more detailed investigations which may coexist with the classification scheme presented above.

The weak-coupling hypothesis states that in order for broken inversion and metallic conductivity to coexist there must be limited coupling between electrons at the Fermi level and the phonon(s) responsible for driving the symmetry-breaking transition [8]. If polar metals exhibiting strong coupling between the Fermi level and the structural distortion were to be discovered, they may deserve separate classification as well. Although TiGaO_3 has been predicted as

a compound that might violate the weak-coupling hypothesis [31], it be would hasty to separately categorize such a material prior to experimental synthesis and characterization. We recently computed the decomposition enthalpy of TiGaO_3 to be about -1 eV/f.u., making it unlikely to be realized in experiment. Studying a series of related ABO_3 compounds ($A = \text{Ti, Zr}$; $B = \text{Al, Ga, In}$) revealed that while each exhibits a dynamically stable polar phase driven by displacements of the A-site cation (which also contributes to the Fermi level), none have a decomposition enthalpy smaller in magnitude than -0.8 eV/f.u.

As was the case with $\text{Sr}_3\text{Sn}_2\text{O}_7$, it seems prudent to primarily concern ourselves with the classification of known compounds, as the synthesis of exotic predicted compounds may reveal features that aid in their classification. Alternatively, we may yet discover factors that prevent the synthesis of acentric conductors that challenge our classification scheme. In the mean time, it is incumbent on theoretical and computational materials scientists to examine the stability of their predicted compounds before sharing their results [118]. At the same time, the high number of superconducting polar metals (Table III) implies that perhaps the description of weak coupling between crystallographic and electronic orders in polar metals is not entirely accurate. There is certainly evidence of a coupled relationship in the degenerately doped superconducting ferroelectrics SrTiO_3 [13,14] and BaTiO_3 [119]. The apparent connection between superconductivity and polar metals (and the associated implications for coupling between the two orders) warrants further investigation.

Accompanying the advent of 2D materials has been a recent interest in the emergent phenomena that occur when two sheets of a material are stacked on top of one another; moiré heterostructures like those in the famous magic angle graphene are being explored in a variety of van der Waals materials [95,120–123]. However, work thus far has exclusively focused on small-band-gap semiconductors and semimetals. In addition, “twisting” typically occurs mechanically and continuously. Concurrently, in the past year we have seen a significant increase in the number of predicted and synthesized two-dimensional polar metals [18,33,124–127]. We see an opportunity to significantly broaden the phase space of both topologically nontrivial materials and acentric conductors by considering two-dimensional metals and scalable, discrete stacking mechanisms.

Metallic correlated transition metal dichalcogenides and halides are just beginning to be investigated in moiré heterostructures. Noting that interlayer twisting at most angles breaks inversion symmetry, this presents a pathway for a new class of noncentrosymmetric metals, which may facilitate the generation of tunable charge density waves, solitons, and phasons, as well as topological conduction mechanisms and create exotic opportunities to support new physics. However, the number of metallic 2D transition metal dichalcogenides is limited, motivating investigations beyond van der Waals stacking (which requires mechanical stacking amidst a continuum of possible twist angles) toward hybrid organic-inorganic materials that can be directly assembled [128,129] or in heteroanionic materials comprising multiple anions [130,131].

As evidenced by Table III, there are a great many predicted compounds; experimental verification of predicted polar met-

als and their properties is a pressing need. In addition, the search for compounds that violate weak coupling continues to be of interest and may require expanding the field into new structure families. Finally, the properties and applications of polar metals are not yet fully appreciated. Recent work on topological phonons indicates that polar metals are ideal candidates to host this recently described phenomenon [132], while the potential for polar metals to impact the fields of photovoltaics [133], energy harvesting [134,135], catalysis [136], microelectronic [137–139], optoelectronic, photonic and plasmonic devices [107,108,140–146], and quantum information systems [147] remains largely untapped.

ACKNOWLEDGMENTS

This work was supported by the Army Research Office (ARO) under Grant No. W911NF-15-1-0017. We thank our numerous colleagues and collaborators for enlightening discussions on polar metals and sharing their laboratory discoveries with us over the last decade.

APPENDIX: ASSUMPTIONS OF THE BACKGROUND-CHARGE APPROXIMATION

The background-charge approach has become the de facto tool for use in studying the effects of electrostatic doping on solid-state materials with density functional theory (DFT) total energy methods [34,57,97,148,149]. This method works by changing the number of electrons present in an electronic structure simulation, while providing an additional homogeneous background charge to maintain charge balance. The background-charge approximation has become popular in doping simulations because it allows one to use smaller unit cells than in substitutional or vacancy-doping simulations and because it allows one to separate the effects of changes in electronic structure from the distortions which accompany real chemical dopants. This is an attractive combination of attributes when studying the interplay between free charge carriers and the polar distortion active in ferroelectrics.

The background-charge method is frequently used both to investigate fundamental relationships and to design polar metals [12,97,148,149]. This approximation, however, has consequences which do not always translate to physical systems. These include, but are not limited to (i) changes in volume; (ii) abrupt changes in conductivity; and (iii) homogeneous changes to electronic and crystallographic structure. Some of these problems are linked to the use of periodic density functional theory (DFT) as a simulation method in general, e.g., (3) can be challenging to avoid while using periodic boundary conditions, and all have been previously observed, but their shortcomings have been amplified by widespread application of the background-charge technique to doped FEs. Despite its limitations, the background-charge approximation remains an extremely valuable method of exploring the effects of doping on electronic and crystallographic structure. The consequences of using this approximation instead of more realistic substitution or vacancy-based doping simulations, however, should be acknowledged to avoid arriving at inaccurate conclusions about the effect of doping in semiconductors and in doped ferroelectrics in particular.

1. Changes in volume

The homogeneous background charge introduced in electrostatic doping simulations produces unintended consequences for the volume of the semiconductor being studied. The effective “pressure” resulting from the additional electrons and associated background is ill defined, resulting in inconsistent consequences depending on the DFT implementation [34]. It follows naturally that this arbitrary treatment of volume leads to results that deviate significantly from experiment. For example, Iwazaki *et al.* showed that volume increases due to electrostatic doping simulations via the background-charge method in BaTiO₃ dramatically overpredicted volume changes as compared to experimental substitutional doping [35]. Volume discrepancies dramatically impact properties, including the stability of the crystal structure, as volume is closely tied to the strength of interatomic forces and hence phonon frequencies. Simulations of soft phonon modes in BaTiO₃ under electrostatic doping with and without volume relaxation produce significantly different critical doping thresholds [57]. If the volume difference between polar and nonpolar phases is substantial, then the volume changes induced by this method will intrinsically favor high- or low-symmetry structures depending on the relative volume [35,97], obfuscating the changes induced by doping. Therefore, it is recommended that electrostatic doping via the compensating background-charge approximation be performed with fixed volume. Volume relaxation may only be used when simulating substitutional, interstitial, or vacancy-based doping. Even in those cases, the dopant concentration should be considered when performing volume relaxations.

2. Abrupt changes in conductivity

In the pristine case, ferroelectric insulators are easily differentiated from metals, both computationally (i.e., gapped band structure) and experimentally (optical conductivity approaches zero at low frequency). Next, the addition of charge carriers can be achieved through chemical means (dopants) or electrostatic gating. Upon chemical substitution, defect states are introduced into the electronic structure of a semiconductor, allowing for modest conductivity due to thermally excited charge carriers occupying the defect states. This may lead to the material exhibiting metal-like temperature-dependent resistivity (i.e., positive slope) away from 0 K, but as temperature is reduced the thermally activated charge carriers are eventually frozen out and resistivity increases. This is reflected in the optical conductivity (σ_0), which still heads to 0 at low frequency [Fig. 2(a)].

Upon additional doping, an impurity band may form, transforming a degenerately doped semiconductor into a bad metal with low mobility from impurity scattering [150,151], as shown schematically in Fig. 7. In this case, the material will exhibit exclusively metallic characteristics, as the impurity band produces a finite σ_0 as $\omega \rightarrow 0$, which can lead to the apparent closure of the gap with sufficient doping as low-frequency spectra weight appears [Fig. 2(a)].

This gradual evolution in conductivity under doping, accompanied by the formation of an impurity band, is not well described using the background-charge method to approximate doping. In real semiconductors, doping shifts the Fermi

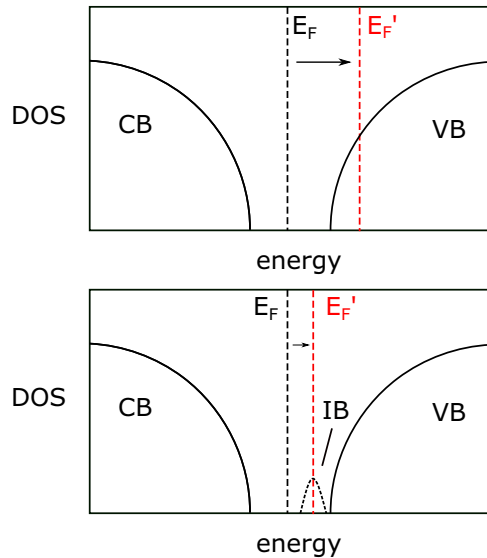


FIG. 7. Schematic illustration of the effect of doping on the electronic structure under the (top) background-charge technique and (bottom) more realistic substitutional doping mechanisms involving the formation of an impurity band (IB).

level up or down within the band gap, but often not to a degree sufficient to push the Fermi level into either the valence or conduction band (Fig. 7). With the background-charge method, even a highly dilute concentration of additional electrons (or holes) is sufficient to place the Fermi level within a band, making the system metallic far below even the electron concentration given by the Mott criterion $n_c^{1/3}a_0 \approx 0.25$ for free electrons, where n_c is the critical carrier density for the transition and a_0 is the effective Bohr radius. Furthermore, the undoped band structure remains more or less intact, precluding the possibility of changes to the electronic structure due to impurity bands or polaron formation (Fig. 7). This simplification obscures the complex reality of changes to the electronic structure that accompany chemical dopants [152].

These changes are highly dependent on choice of starting material and doping method (substitution, vacancy, electrostatic, etc.). The critical charge-carrier concentration (n^*) for conductivity in BaTiO_3 alone varies considerably across several doping mechanisms [15,41,153], all of which are significantly higher than n^* for SrTiO_3 [154]. The background-charge method is not able to account for these differences and therefore may lead to misleading conclusions about the ease of altering the conductivity of a material. It may come closest to approximating electrostatic gating, as this field-driven method typically does not generate an impurity band. However, it still ignores charge localization mechanisms discussed next.

3. Homogeneous changes to crystallographic and electronic structure

Below the impurity band formation limit, or under electrostatic gating, the carriers will either be homogeneously or inhomogeneously distributed at the nanoscale. At present, nearly all DFT calculations make the assumption that carriers are homogeneously distributed, and by construction the simulations result in a metallic electronic structure. Whether or not this model accurately captures the experimental situation requires attention, as recent extensions of semiconductor doping principles to transition metal compounds show that homogeneous distributions are often the exception rather than the rule [155].

For the inhomogeneous case, we anticipate nanoscale phase segregation to occur in close analogy to what happens across metal-insulator phase transitions in complex oxides such as VO_2 [156]. Here doping leads to domains that are either metallic or insulating and local structures that are centrosymmetric and noncentrosymmetric, respectively. In other words, the regions that are metallic recover inversion while inversion symmetry remains lifted in the insulating regions. This electronic- and parity-symmetry phase separation is supported by recent studies on BaTiO_3 and SrTiO_3 [153,154]. Indeed, BaTiO_3 is much more difficult to make metallic than SrTiO_3 [154] with the key difference being the lattice dynamical properties; BaTiO_3 is a soft-mode semiconducting ferroelectric whereas SrTiO_3 is an incipient ferroelectric with a highly dilute superconducting transition. In practice this means that long-range order quickly breaks down in doped BaTiO_3 , as the driving force for local off centering persists leading to a network of disordered insulating octahedra separated by centrosymmetric metallic clusters hosting pseudolocalized free charge carriers. By contrast, under similar doping conditions, the more regular octahedra of SrTiO_3 enter a metallic, and subsequently superconducting, state. SrTiO_3 is not immune to nanodomain formation [157], but charge does not localize as easily. This highlights the fact that the experimental structure may exhibit electronic structure heterogeneities in real space with regard to either the electronic structure and/or crystal structure.

Meanwhile, nearly all DFT calculations assume homogeneous doping. This is unavoidable to a certain extent, due to the prohibitive cost of simulating the large supercells necessary to capture nanodomain structures on the mesoscale. However, the background-charge method further enforces uniformity, as the added charge carriers are distributed among the bands closest to the Fermi level while a homogeneous compensating background charge is added for charge balance. This makes it very challenging to simulate localization or polaron formation, let alone account for multiple phases.

[1] P. W. Anderson and E. I. Blount, Symmetry Considerations on Martensitic Transformations: “Ferroelectric” Metals? *Phys. Rev. Lett.* **14**, 217 (1965).

[2] E. K. Salje, Ferroelastic materials, *Annu. Rev. Mater. Res.* **42**, 265 (2012).

[3] J. L. de Lagrange, Sur l’attraction des sphéroïdes elliptiques, *Nouv. Mém. Acad. Royale Berlin année 3*, 619 (1773).

- [4] C. F. Gauss, *Theoria attractionis corporum sphaeroidicorum ellipticorum homogeneorum*, in *Werke* (Springer, Berlin, 1877), pp. 3–22.
- [5] W. Cochran, Crystal Stability and the Theory of Ferroelectricity, *Phys. Rev. Lett.* **3**, 412 (1959).
- [6] R. E. Cohen, Origin of ferroelectricity in perovskite oxides, *Nature (London)* **358**, 136 (1992).
- [7] Y. Shi, Y. Guo, X. Wang, A. J. Princep, D. Khalyavin, P. Manuel, Y. Michiue, A. Sato, K. Tsuda, S. Yu, M. Arai, Y. Shirako, M. Akaogi, N. Wang, K. Yamaura, and A. T. Boothroyd, A ferroelectric-like structural transition in a metal, *Nat. Mater.* **12**, 1024 (2013).
- [8] D. Puggioni and J. M. Rondinelli, Designing a robustly metallic noncentrosymmetric ruthenate oxide with large thermopower anisotropy, *Nat. Commun.* **5**, 3432 (2014).
- [9] D. Varjas, A. G. Grushin, R. Ilan, and J. E. Moore, Dynamical Piezoelectric and Magnetopiezoelectric Effects in Polar Metals from Berry Phases and Orbital Moments, *Phys. Rev. Lett.* **117**, 257601 (2016).
- [10] L. Wu, S. Patankar, T. Morimoto, N. L. Nair, E. Thewalt, A. Little, J. G. Analytis, J. E. Moore, and J. Orenstein, Giant anisotropic nonlinear optical response in transition metal monpnictide Weyl semimetals, *Nat. Phys.* **13**, 350 (2017).
- [11] H. Gao, Y. Kim, J. W. F. Venderbos, C. L. Kane, E. J. Mele, A. M. Rappe, and W. Ren, Dirac-Weyl Semimetal: Coexistence of Dirac and Weyl Fermions in Polar Hexagonal ABC Crystals, *Phys. Rev. Lett.* **121**, 106404 (2018).
- [12] X. He and K. Juan Jin, Persistence of polar distortion with electron doping in lone-pair driven ferroelectrics, *Phys. Rev. B* **94**, 224107 (2016).
- [13] K. Ahadi, L. Galletti, Y. Li, S. Salmani-Rezaie, W. Wu, and S. Stemmer, Enhancing superconductivity in SrTiO₃ films with strain, *Sci. Adv.* **5**, eaaw0120 (2019).
- [14] J. F. Schooley, W. R. Hosler, and M. L. Cohen, Superconductivity in Semiconducting SrTiO₃, *Phys. Rev. Lett.* **12**, 474 (1964).
- [15] T. Kolodiaznyy, M. Tachibana, H. Kawaji, J. Hwang, and E. Takayama-Muromachi, Persistence of Ferroelectricity in BaTiO₃ Through the Insulator-Metal Transition, *Phys. Rev. Lett.* **104**, 147602 (2010).
- [16] S. Lei, M. Gu, D. Puggioni, G. Stone, J. Peng, J. Ge, Y. Wang, B. Wang, Y. Yuan, K. Wang, Z. Mao, J. M. Rondinelli, and V. Gopalan, Observation of quasi-two-dimensional polar domains and ferroelastic switching in a metal, Ca₃Ru₂O₇, *Nano Lett.* **18**, 3088 (2018).
- [17] Y. Yoshida, S.-I. Ikeda, H. Matsuhata, N. Shirakawa, C. H. Lee, and S. Katano, Crystal and magnetic structure of Ca₃Ru₂O₇, *Phys. Rev. B* **72**, 054412 (2005).
- [18] Z. Fei, W. Zhao, T. A. Palomaki, B. Sun, M. K. Miller, Z. Zhao, J. Yan, X. Xu, and D. H. Cobden, Ferroelectric switching of a two-dimensional metal, *Nature (London)* **560**, 336 (2018).
- [19] H. Zheng, B. C. Wilfong, D. Hickox-Young, J. M. Rondinelli, P. Y. Zavalij, and E. E. Rodriguez, Polar ferromagnetic metal by intercalation of metal-amine complexes, *Chem. Mater.* **33**, 4936 (2021).
- [20] A. J. E. Rettie, C. D. Malliakas, A. S. Botana, J.-K. Bao, D. Y. Chung, and M. G. Kanatzidis, KCu₇P₃: A two-dimensional noncentrosymmetric metallic pnictide, *Inorg. Chem.* **58**, 10201 (2019).
- [21] N. A. Benedek and T. Birol, ‘ferroelectric’ metals reexamined: fundamental mechanisms and design considerations for new materials, *J. Mater. Chem. C* **4**, 4000 (2016).
- [22] W. X. Zhou and A. Ariando, Review on ferroelectric/polar metals, *Jpn. J. Appl. Phys.* **59**, S10802 (2020).
- [23] S. Bhowal and N. A. Spaldin, Polar metals: Principles and prospects, [arXiv:2210.02993](https://arxiv.org/abs/2210.02993).
- [24] J. Nye and P. Nye, *Physical Properties of Crystals: Their Representation by Tensors and Matrices*, Oxford Science Publications (Clarendon, Oxford, 1985).
- [25] S. Baroni, P. Giannozzi, and A. Testa, Green’s-Function Approach to Linear Response in Solids, *Phys. Rev. Lett.* **58**, 1861 (1987).
- [26] R. Resta, Macroscopic electric polarization as a geometric quantum phase, *Europhys. Lett.* **22**, 133 (1993).
- [27] R. D. King-Smith and D. Vanderbilt, Theory of polarization of crystalline solids, *Phys. Rev. B* **47**, 1651 (1993).
- [28] D. Vanderbilt, *Berry Phases in Electronic Structure Theory: Electric Polarization, Orbital Magnetization and Topological Insulators* (Cambridge University Press, Cambridge, 2018).
- [29] R. E. Cohen and H. Krakauer, Lattice dynamics and origin of ferroelectricity in BaTiO₃: Linearized-augmented-plane-wave total-energy calculations, *Phys. Rev. B* **42**, 6416 (1990).
- [30] J.-x. Gu, K.-j. Jin, C. Ma, Q.-h. Zhang, L. Gu, C. Ge, J.-s. Wang, C. Wang, H.-Z. Guo, and G.-Z. Yang, Coexistence of polar distortion and metallicity in PbTi_{1-x}Nb_xO₃, *Phys. Rev. B* **96**, 165206 (2017).
- [31] H. J. Xiang, Origin of polar distortion in LiNbO₃-type “ferroelectric” metals: Role of A-site instability and short-range interactions, *Phys. Rev. B* **90**, 094108 (2014).
- [32] F. Jin, A. Zhang, J. Ji, K. Liu, L. Wang, Y. Shi, Y. Tian, X. Ma, and Q. Zhang, Raman phonons in the ferroelectric-like metal LiOsO₃, *Phys. Rev. B* **93**, 064303 (2016).
- [33] A. Filippetti, V. Fiorentini, F. Ricci, P. Delugas, and J. Íñiguez, Prediction of a native ferroelectric metal, *Nat. Commun.* **7**, 11211 (2016).
- [34] F. Bruneval, C. Varvenne, J.-P. Crocombette, and E. Clouet, Pressure, relaxation volume, and elastic interactions in charged simulation cells, *Phys. Rev. B* **91**, 024107 (2015).
- [35] Y. Iwazaki, T. Suzuki, Y. Mizuno, and S. Tsuneyuki, Doping-induced phase transitions in ferroelectric BaTiO₃ from first-principles calculations, *Phys. Rev. B* **86**, 214103 (2012).
- [36] J. F. Scott, Ferroelectrics go bananas, *J. Phys.: Condens. Matter* **20**, 021001 (2008).
- [37] W. Kohn, Theory of the insulating state, *Phys. Rev.* **133**, A171 (1964).
- [38] P. P. Edwards, M. T. Lodge, F. Hensel, and R. Redmer, ‘... a metal conducts and a non-metal doesn’t’, *Philos. Trans. R. Soc. London A* **368**, 941 (2010).
- [39] P. P. Edwards, in *Nevill Mott: Reminiscences and Appreciations*, edited by E. A. Davis (CRC Press, Boca Raton, FL, 1998).
- [40] K. S. Takahashi, Y. Matsubara, M. S. Bahramy, N. Ogawa, D. Hashizume, Y. Tokura, and M. Kawasaki, Polar metal phase stabilized in strained La-doped BaTiO₃ films, *Sci. Rep.* **7**, 4631 (2017).
- [41] J. Fujioka, A. Doi, D. Okuyama, D. Morikawa, T. Arima, K. N. Okada, Y. Kaneko, T. Fukuda, H. Uchiyama, D. Ishikawa, A. Q. R. Baron, K. Kato, M. Takata, and Y. Tokura,

- Ferroelectric-like metallic state in electron doped BaTiO₃, *Sci. Rep.* **5**, 13207 (2015).
- [42] T. Kolodiazny, Insulator-metal transition and anomalous sign reversal of the dominant charge carriers in perovskite BaTiO_{3- δ} , *Phys. Rev. B* **78**, 045107 (2008).
- [43] D. J. Scalapino, S. R. White, and S. Zhang, Insulator, metal, or superconductor: The criteria, *Phys. Rev. B* **47**, 7995 (1993).
- [44] R. Resta, Why are insulators insulating and metals conducting? *J. Phys.: Condens. Matter* **14**, R625 (2002).
- [45] N. W. Ashcroft and N. D. Mermin, *Solid State Physics* (Dover, New York, 1976).
- [46] F. Bloch, Zum elektrischen widerstandsgesetz bei tiefen temperaturen, *Z. Phys.* **59**, 208 (1930).
- [47] E. Grüneisen, Die abhängigkeit des elektrischen widerstandes reiner metalle von der temperatur, *Ann. Phys. (Berlin)* **408**, 530 (1933).
- [48] Y. Yoshida, I. Nagai, S.-I. Ikeda, N. Shirakawa, M. Kosaka, and N. Môri, Quasi-two-dimensional metallic ground state of Ca₃Ru₂O₇, *Phys. Rev. B* **69**, 220411(R) (2004).
- [49] J. Hwang, T. Kolodiazny, J. Yang, and M. Couillard, Doping and temperature-dependent optical properties of oxygen-reduced BaTiO_{3- δ} , *Phys. Rev. B* **82**, 214109 (2010).
- [50] A. J. Millis and S. N. Coppersmith, Variational wave functions and the Mott transition, *Phys. Rev. B* **43**, 13770 (1991).
- [51] C. C. Homes, T. Timusk, R. Liang, D. A. Bonn, and W. N. Hardy, Optical Conductivity of c Axis Oriented YBa₂Cu₃O_{6.70}: Evidence for a Pseudogap, *Phys. Rev. Lett.* **71**, 1645 (1993).
- [52] C. E. Dreyer, S. Coh, and M. Stengel, Nonadiabatic Born Effective Charges in Metals and the Drude Weight, *Phys. Rev. Lett.* **128**, 095901 (2022).
- [53] W. E. Anderson, R. W. Alexander, and R. J. Bell, Surface Plasmons and the Reflectivity of n-Type InSb, *Phys. Rev. Lett.* **27**, 1057 (1971).
- [54] C. Z. Bi, J. Y. Ma, J. Yan, X. Fang, B. R. Zhao, D. Z. Yao, and X. G. Qiu, Electron-phonon coupling in Nb-doped SrTiO₃ single crystal, *J. Phys.: Condens. Matter* **18**, 2553 (2006).
- [55] I. Iovcchio, G. Giovannetti, M. Autore, P. DiPietro, A. Perucchi, J. He, K. Yamaura, M. Capone, and S. Lupi, Electronic correlations in the ferroelectric metallic state of LiOsO₃, *Phys. Rev. B* **93**, 161113(R) (2016).
- [56] I. B. Bersuker, Pseudo-Jahn-Teller effect—A two-state paradigm in formation, deformation, and transformation of molecular systems and solids, *Chem. Rev.* **113**, 1351 (2013).
- [57] D. Hickox-Young, D. Puggioni, and J. M. Rondinelli, Persistent polar distortions from covalent interactions in doped BaTiO₃, *Phys. Rev. B* **102**, 014108 (2020).
- [58] P. Ghosez, X. Gonze, and J.-P. Michenaud, Coulomb interaction and ferroelectric instability of BaTiO₃, *Europhys. Lett.* **33**, 713 (1996).
- [59] S. Salmani-Rezaie, K. Ahadi, W. M. Strickland, and S. Stemmer, Order-disorder ferroelectric transition of strained SrTiO₃, *Phys. Rev. Lett.* **125**, 087601 (2020).
- [60] C. Chepkemboi, K. Jorgensen, J. Sato, and G. Laurita, Strategies and considerations for least-squares analysis of total scattering data, *ACS Omega* **7**, 14402 (2022).
- [61] G. Giovannetti, D. Puggioni, J. M. Rondinelli, and M. Capone, Interplay between electron correlations and polar displacements in metallic SrEuMo₂O₆, *Phys. Rev. B* **93**, 115147 (2016).
- [62] D. Puggioni, G. Giovannetti, M. Capone, and J. M. Rondinelli, Design of a Mott Multiferroic from a Nonmagnetic Polar Metal, *Phys. Rev. Lett.* **115**, 087202 (2015).
- [63] S. Mülbauer, B. Binz, F. Jonietz, C. Pfleiderer, A. Rosch, A. Neubauer, R. Georgii, and P. Böni, Skyrmion lattice in a chiral magnet, *Science* **323**, 915 (2009).
- [64] T. Schulz, R. Ritz, A. Bauer, M. Halder, M. Wagner, C. Franz, C. Pfleiderer, K. Everschor, M. Garst, and A. Rosch, Emergent electrodynamics of skyrmions in a chiral magnet, *Nat. Phys.* **8**, 301 (2012).
- [65] X. Z. Yu, Y. Onose, N. Kanazawa, J. H. Park, J. H. Han, Y. Matsui, N. Nagaosa, and Y. Tokura, Real-space observation of a two-dimensional skyrmion crystal, *Nature (London)* **465**, 901 (2010).
- [66] S.-W. Cheong and X. Xu, Magnetic chirality, *npj Quantum Mater.* **7**, 40 (2022).
- [67] An american national standard IEEE standard definitions of terms associated with ferroelectric and related materials, *IEEE Transactions Ultrasonics, Ferroelect. Freq. Control* **50**, 1 (2003).
- [68] K. Aizu, Possible species of “ferroelastic crystals and of simultaneously ferroelectric and ferroelastic crystals, *J. Phys. Soc. Jpn.* **27**, 387 (1969).
- [69] H. Sakai, K. Ikeura, M. S. Bahramy, N. Ogawa, D. Hashizume, J. Fujioka, Y. Tokura, and S. Ishiwata, Critical enhancement of thermopower in a chemically tuned polar semimetal MoTe₂, *Sci. Adv.* **2**, e1601378 (2016).
- [70] F. Jin, L. Wang, A. Zhang, J. Ji, Y. Shi, X. Wang, R. Yu, J. Zhang, E. W. Plummer, and Q. Zhang, Raman interrogation of the ferroelectric phase transition in polar metal LiOsO₃, *Proc. Natl. Acad. Sci. USA* **116**, 20322 (2019).
- [71] G. Stone, D. Puggioni, S. Lei, M. Gu, K. Wang, Y. Wang, J. Ge, X.-Z. Lu, Z. Mao, J. M. Rondinelli, and V. Gopalan, Atomic and electronic structure of domains walls in a polar metal, *Phys. Rev. B* **99**, 014105 (2019).
- [72] T. H. Kim, D. Puggioni, Y. Yuan, L. Xie, H. Zhou, N. Campbell, P. J. Ryan, Y. Choi, J.-W. Kim, J. R. Patzner, S. Ryu, J. P. Podkaminer, J. Irwin, Y. Ma, C. J. Fennie, M. S. Rzchowski, X. Q. Pan, V. Gopalan, J. M. Rondinelli, and C. B. Eom, Polar metals by geometric design, *Nature (London)* **533**, 68 (2016).
- [73] H. Padmanabhan, Y. Park, D. Puggioni, Y. Yuan, Y. Cao, L. Gasparov, Y. Shi, J. Chakhalian, J. M. Rondinelli, and V. Gopalan, Linear and nonlinear optical probe of the ferroelectric-like phase transition in a polar metal, LiOsO₃, *Appl. Phys. Lett.* **113**, 122906 (2018).
- [74] N. J. Laurita, A. Ron, J.-Y. Shan, D. Puggioni, N. Z. Koocher, K. Yamaura, Y. Shi, J. M. Rondinelli, and D. Hsieh, Evidence for the weakly coupled electron mechanism in an Anderson-Blount polar metal, *Nat. Commun.* **10**, 3217 (2019).
- [75] V. K. Wadhawan, Ferroelasticity, *Bulletin Materials Science* **6**, 733 (1984).
- [76] G. Slosarek, A. Heuer, H. Zimmermann, and U. Haebleren, A study of the paraelectric-ferroelectric phase transition of triglycine sulphate by deuteron nuclear magnetic resonance and relaxation, *J. Phys.: Condens. Matter* **1**, 5931 (1989).

- [77] V. Gopalan, V. Dierolf, and D. A. Scrymgeour, Defect–domain wall interactions in trigonal ferroelectrics, *Annu. Rev. Mater. Res.* **37**, 449 (2007).
- [78] K. Shapovalov, P. Yudin, A. Tagantsev, E. Eliseev, A. Morozovska, and N. Setter, Elastic Coupling between Nonferroelastic Domain Walls, *Phys. Rev. Lett.* **113**, 207601 (2014).
- [79] Y.-W. Fang and H. Chen, Design of a multifunctional polar metal via first-principles high-throughput structure screening, *Commun. Mater.* **1**, 1 (2020).
- [80] H. Watanabe and Y. Yanase, Magnetic hexadecapole order and magnetopiezoelectric metal state in $\text{Ba}_{1-x}\text{K}_x\text{Mn}_2\text{As}_2$, *Phys. Rev. B* **96**, 064432 (2017).
- [81] <https://mtd.mccormick.northwestern.edu/polar-metals-materials-database/>
- [82] E. Bauer, G. Hilscher, H. Michor, C. Paul, E. W. Scheidt, A. Gribanov, Y. Seropegin, H. No'el, M. Sigrist, and P. Rogl, Heavy Fermion Superconductivity and Magnetic Order in Noncentrosymmetric CePt_3Si , *Phys. Rev. Lett.* **92**, 027003 (2004).
- [83] Y. Jiao, Y.-W. Fang, J. Sun, P. Shan, Z. Yu, H. L. Feng, B. Wang, H. Ma, Y. Uwatoko, K. Yamaura, Y. Guo, H. Chen, and J. Cheng, Coupled magnetic and structural phase transitions in the antiferromagnetic polar metal $\text{Pb}_2\text{CoOsO}_6$ under pressure, *Phys. Rev. B* **102**, 144418 (2020).
- [84] C. W. Rischau, X. Lin, C. P. Grams, D. Finck, S. Harms, J. Engelmayer, T. Lorenz, Y. Gallais, B. Fauqué, J. Hemberger, and K. Behnia, A ferroelectric quantum phase transition inside the superconducting dome of $\text{Sr}_{1-x}\text{Ca}_x\text{TiO}_{3-\delta}$, *Nat. Phys.* **13**, 643 (2017).
- [85] E. Berger, S. Jamnuch, C. B. Uzundal, C. Woodahl, H. Padmanabhan, A. Amado, P. Manset, Y. Hirata, Y. Kubota, S. Owada, K. Tono, M. Yabashi, C. Wang, Y. Shi, V. Gopalan, C. P. Schwartz, W. S. Drisdell, I. Matsuda, J. W. Freeland, T. A. Pascal *et al.*, Extreme ultraviolet second harmonic generation spectroscopy in a polar metal, *Nano Lett.* **21**, 6095 (2021).
- [86] Y. Pan, A. M. Nikitin, T. V. Bay, Y. K. Huang, C. Paulsen, B. H. Yan, and A. de Visser, Superconductivity and magnetic order in the noncentrosymmetric half-Heusler compound ErPdBi , *Europhys. Lett.* **104**, 27001 (2013).
- [87] J. Jiang, Z. L. Bai, Z. H. Chen, L. He, D. W. Zhang, Q. H. Zhang, J. A. Shi, M. H. Park, J. F. Scott, C. S. Hwang, and A. Q. Jiang, Temporary formation of highly conducting domain walls for non-destructive read-out of ferroelectric domain-wall resistance switching memories, *Nat. Mater.* **17**, 49 (2018).
- [88] T. Choi, Y. Horibe, H. T. Yi, Y. J. Choi, W. Wu, and S.-W. Cheong, Insulating interlocked ferroelectric and structural antiphase domain walls in multiferroic YMnO_3 , *Nat. Mater.* **9**, 253 (2010).
- [89] K. Jiang, R. Zhao, P. Zhang, Q. Deng, J. Zhang, W. Li, Z. Hu, H. Yang, and J. Chu, Strain and temperature dependent absorption spectra studies for identifying the phase structure and band gap of EuTiO_3 perovskite films, *Phys. Chem. Chem. Phys.* **17**, 31618 (2015).
- [90] T. S. Holstad, T. M. Ræder, D. M. Evans, D. R. Småbråten, S. Krohns, J. Schaab, Z. Yan, E. Bourret, A. T. J. van Helvoort, T. Grande, S. M. Selbach, J. C. Agar, and D. Meier, Application of a long short-term memory for deconvoluting conductance contributions at charged ferroelectric domain walls, *npj Comput. Mater.* **6**, 163 (2020).
- [91] C. Cantoni, J. Gazquez, F. M. Granozio, M. P. Oxley, M. Varela, A. R. Lupini, S. J. Pennycook, C. Aruta, U. S. di Uccio, P. Perna, and D. Maccariello, Electron transfer and ionic displacements at the origin of the 2d electron gas at the LAO/STO interface: Direct measurements with atomic-column spatial resolution, *Adv. Mater.* **24**, 3952 (2012).
- [92] J. Bréhin, F. Trier, L. M. Vicente-Arche, P. Hemme, P. Noël, M. Cosset-Chéneau, J.-P. Attané, L. Vila, A. Sander, Y. Gallais, A. Sacuto, B. Dkhil, V. Garcia, S. Fusil, A. Barthélémy, M. Cazayous, and M. Bibes, Switchable two-dimensional electron gas based on ferroelectric Ca:SrTiO_3 , *Phys. Rev. Mater.* **4**, 041002(R) (2020).
- [93] P. Noël, F. Trier, L. M. V. Arche, J. Bréhin, D. C. Vaz, V. Garcia, S. Fusil, A. Barthélémy, L. Vila, M. Bibes, and J.-P. Attané, Non-volatile electric control of spin–charge conversion in a SrTiO_3 rashba system, *Nature (London)* **580**, 483 (2020).
- [94] J. Bréhin, Y. Chen, M. D'Antuono, S. Varotto, D. Stornaiuolo, C. Piamonteze, J. Varignon, M. Salluzzo, and M. Bibes, A multiferroic two-dimensional electron gas, [arXiv:2206.03843](https://arxiv.org/abs/2206.03843).
- [95] Y. Cao, V. Fatemi, S. Fang, K. Watanabe, T. Taniguchi, E. Kaxiras, and P. Jarillo-Herrero, Unconventional superconductivity in magic-angle graphene superlattices, *Nature (London)* **556**, 43 (2018).
- [96] W. X. Zhou, H. J. Wu, J. Zhou, S. W. Zeng, C. J. Li, M. S. Li, R. Guo, J. X. Xiao, Z. Huang, W. M. Lv, K. Han, P. Yang, C. G. Li, Z. S. Lim, H. Wang, Y. Zhang, S. J. Chua, K. Y. Zeng, T. Venkatesan, J. S. Chen *et al.*, Artificial two-dimensional polar metal by charge transfer to a ferroelectric insulator, *Commun. Phys.* **2**, 125 (2019).
- [97] H. J. Zhao, A. Filippetti, C. Escorihuela-Sayalero, P. Delugas, E. Canadell, L. Bellaïche, V. Fiorentini, and J. Íñiguez, Meta-screening and permanence of polar distortion in metallized ferroelectrics, *Phys. Rev. B* **97**, 054107 (2018).
- [98] S. Lee, R. H. T. Wilke, S. Trolrier-McKinstry, S. Zhang, and C. A. Randall, $\text{Sr}_x\text{Ba}_{1-x}\text{Nb}_2\text{O}_{6-\delta}$ ferroelectric-thermoelectrics: Crystal anisotropy, conduction mechanism, and power factor, *Appl. Phys. Lett.* **96**, 031910 (2010).
- [99] S. Lee, J. A. Bock, S. Trolrier-McKinstry, and C. A. Randall, Ferroelectric-thermoelectricity and Mott transition of ferroelectric oxides with high electronic conductivity, *J. Eur. Ceram. Soc.* **32**, 3971 (2012).
- [100] A. Banik, T. Ghosh, R. Arora, M. Dutta, J. Pandey, S. Acharya, A. Soni, U. V. Waghmare, and K. Biswas, Engineering ferroelectric instability to achieve ultralow thermal conductivity and high thermoelectric performance in $\text{Sn}_{1-x}\text{Ge}_x\text{Te}$, *Energy Environ. Sci.* **12**, 589 (2019).
- [101] D. Dangić, S. Fahy, and I. Savić, Giant thermoelectric power factor in charged ferroelectric domain walls of GeTe with van Hove singularities, *npj Comput. Mater.* **6**, 195 (2020).
- [102] T. Nakajima, H. Oike, A. Kikkawa, E. P. Gilbert, N. Booth, K. Kakurai, Y. Taguchi, Y. Tokura, F. Kagawa, and T. Hisa Arima, Skyrmion lattice structural transition in MnSi , *Sci. Adv.* **3**, e1602562 (2017).
- [103] Y. Zhou and K. M. Rabe, Coupled Nonpolar-Polar Metal-Insulator Transition in $\text{SrCrO}_3/\text{SrTiO}_3$ Superlattices: A First-Principles Study, *Phys. Rev. Lett.* **115**, 106401 (2015).

- [104] Y. Zhang, J.-J. Gong, C.-F. Li, L. Lin, Z.-B. Yan, S. Dong, and J.-M. Liu, Strain-Induced Slater Transition in Polar Metal LiOsO_3 , *Phys. Status Solidi RRL* **13**, 1900436 (2019).
- [105] S. Li and T. Birol, Free-Carrier-Induced Ferroelectricity in Layered Perovskites, *Phys. Rev. Lett.* **127**, 087601 (2021).
- [106] T. Cao, G. Ren, D.-F. Shao, E. Y. Tsymlal, and R. Mishra, Stabilizing polar phases in binary metal oxides by hole doping, [arXiv:2209.09436](https://arxiv.org/abs/2209.09436).
- [107] K. Nisi, S. Subramanian, W. He, K. A. Ulman, H. El-Sherif, F. Sigger, M. Lassaunière, M. T. Wetherington, N. Briggs, J. Gray, A. W. Holleitner, N. Bassim, S. Y. Quek, J. A. Robinson, and U. Wurstbauer, Light-matter interaction in quantum confined 2D polar metals, *Adv. Funct. Mater.* **31**, 2005977 (2021).
- [108] M. A. Steves, Y. Wang, N. Briggs, T. Zhao, H. El-Sherif, B. M. Bersch, S. Subramanian, C. Dong, T. Bowen, A. D. L. F. Duran, K. Nisi, M. Lassaunière, U. Wurstbauer, N. D. Bassim, J. Fonseca, J. T. Robinson, V. H. Crespi, J. Robinson, and K. L. K. Jr, Unexpected near-infrared to visible nonlinear optical properties from 2-D polar metals, *Nano Lett.* **20**, 8312 (2020).
- [109] H. L. Feng, C.-J. Kang, P. Manuel, F. Orlandi, Y. Su, J. Chen, Y. Tsujimoto, J. Hadermann, G. Kotliar, K. Yamaura, E. E. McCabe, and M. Greenblatt, Antiferromagnetic order breaks inversion symmetry in a metallic double perovskite, $\text{Pb}_2\text{NiOsO}_6$, *Chem. Mater.* **33**, 4188 (2021).
- [110] S. Salmani-Rezaie, L. Galletti, T. Schumann, R. Russell, H. Jeong, Y. Li, J. W. Harter, and S. Stemmer, Superconductivity in magnetically doped SrTiO_3 , *Appl. Phys. Lett.* **118**, 202602 (2021).
- [111] H. Jacobsen, H. L. Feng, A. J. Princep, M. C. Rahn, Y. Guo, J. Chen, Y. Matsushita, Y. Tsujimoto, M. Nagao, D. Khalyavin, P. Manuel, C. A. Murray, C. Donnerer, J. G. Vale, M. M. Sala, K. Yamaura, and A. T. Boothroyd, Magnetically induced metal-insulator transition in $\text{Pb}_2\text{CaOsO}_6$, *Phys. Rev. B* **102**, 214409 (2020).
- [112] M. Zhu, J. Peng, W. Tian, T. Hong, Z. Q. Mao, and X. Ke, Tuning the competing phases of bilayer ruthenate $\text{Ca}_3\text{Ru}_2\text{O}_7$ via dilute Mn impurities and magnetic field, *Phys. Rev. B* **95**, 144426 (2017).
- [113] S. Lei, S. Chikara, D. Puggioni, J. Peng, M. Zhu, M. Gu, W. Zhao, Y. Wang, Y. Yuan, H. Akamatsu, M. H. W. Chan, X. Ke, Z. Mao, J. M. Rondinelli, M. Jaime, J. Singleton, F. Weickert, V. S. Zapf, and V. Gopalan, Comprehensive magnetic phase diagrams of the polar metal $\text{Ca}_3(\text{Ru}_{0.95}\text{Fe}_{0.05})_2\text{O}_7$, *Phys. Rev. B* **99**, 224411 (2019).
- [114] S. Tsuda, N. Kikugawa, K. Sugii, S. Uji, S. Ueda, M. Nishio, and Y. Maeno, Mott transition extremely sensitive to impurities in $\text{Ca}_3\text{Ru}_2\text{O}_7$ revealed by hard x-ray photoemission studies, *Phys. Rev. B* **87**, 241107(R) (2013).
- [115] D. Puggioni, M. Horio, J. Chang, and J. M. Rondinelli, Cooperative interactions govern the fermiology of the polar metal $\text{Ca}_3\text{Ru}_2\text{O}_7$, *Phys. Rev. Res.* **2**, 023141 (2020).
- [116] X. Ke, J. Peng, W. Tian, T. Hong, M. Zhu, and Z. Q. Mao, Commensurate-incommensurate magnetic phase transition in the Fe-doped bilayer ruthenate $\text{Ca}_3\text{Ru}_2\text{O}_7$, *Phys. Rev. B* **89**, 220407(R) (2014).
- [117] J. Peng, X. M. Gu, G. T. Zhou, W. Wang, J. Y. Liu, Y. Wang, Z. Q. Mao, X. S. Wu, and S. Dong, Electron mass enhancement and magnetic phase separation near the mott transition in double-layer ruthenates, *Front. Phys.* **13**, 137108 (2018).
- [118] O. I. Malyi, G. M. Dalpian, X.-G. Zhao, Z. Wang, and A. Zunger, Realization of predicted exotic materials: The burden of proof, *Mater. Today* **32**, 35 (2020).
- [119] J. Ma, R. Yang, and H. Chen, A large modulation of electron-phonon coupling and an emergent superconducting dome in doped strong ferroelectrics, *Nat. Commun.* **12**, 2314 (2021).
- [120] D. M. Kennes, M. Claassen, L. Xian, A. Georges, A. J. Millis, J. Hone, C. R. Dean, D. N. Basov, A. N. Pasupathy, and A. Rubio, Moiré heterostructures as a condensed-matter quantum simulator, *Nat. Phys.* **17**, 155 (2021).
- [121] M. A. Susner, M. Chyasnachyus, M. A. McGuire, P. Ganesh, and P. Maksymovych, Metal thio- and selenophosphates as multifunctional van der Waals layered materials, *Adv. Mater.* **29**, 1602852 (2017).
- [122] K. F. Mak, J. Shan, and D. C. Ralph, Probing and controlling magnetic states in 2D layered magnetic materials, *Nat. Rev. Phys.* **1**, 646 (2019).
- [123] C. Gong and X. Zhang, Two-dimensional magnetic crystals and emergent heterostructure devices, *Science* **363**, eaav4450 (2019).
- [124] T. Xu, J. Zhang, Y. Zhu, J. Wang, T. Shimada, T. Kitamura, and T.-Y. Zhang, Two-dimensional polar metal of a PbTe monolayer by electrostatic doping, *Nanoscale Horizons* **5**, 1400 (2020).
- [125] M. Ye, S. Hu, S. Ke, Y. Zhu, Y. Zhang, L. Xie, Y. Zhang, D. Zhang, Z. Luo, M. Gu, J. He, P. Zhang, W. Zhang, and L. Chen, Observation of a room temperature two-dimensional ferroelectric metal, [arXiv:1908.08726](https://arxiv.org/abs/1908.08726).
- [126] W. Luo, K. Xu, and H. Xiang, Two-dimensional hyperferroelectric metals: A different route to ferromagnetic-ferroelectric multiferroics, *Phys. Rev. B* **96**, 1235415 (2017).
- [127] J. Lu, G. Chen, W. Luo, J. Ñíguez, L. Bellaiche, and H. Xiang, Ferroelectricity with Asymmetric Hysteresis in Metallic LiOsO_3 Ultrathin Films, *Phys. Rev. Lett.* **122**, 227601 (2019).
- [128] H. L. B. Boström, M. S. Senn, and A. L. Goodwin, Recipes for improper ferroelectricity in molecular perovskites, *Nat. Commun.* **9**, 2380 (2018).
- [129] M. L. Aubrey, A. S. Valdes, M. R. Filip, B. A. Connor, K. P. Lindquist, J. B. Neaton, and H. I. Karunadasa, Directed assembly of layered perovskite heterostructures as single crystals, *Nature (London)* **597**, 355 (2021).
- [130] H. Kageyama, K. Hayashi, K. Maeda, J. P. Attfield, Z. Hiroi, J. M. Rondinelli, and K. R. Poeppelmeier, Expanding frontiers in materials chemistry and physics with multiple anions, *Nat. Commun.* **9**, 772 (2018).
- [131] J. K. Harada, N. Charles, K. R. Poeppelmeier, and J. M. Rondinelli, Heteroanionic materials by design: Progress toward targeted properties, *Adv. Mater.* **31**, 1805295 (2019).
- [132] B. Peng, Y. Hu, S. Murakami, T. Zhang, and B. Monserrat, Topological phonons in oxide perovskites controlled by light, *Sci. Adv.* **6**, eabd1618 (2020).
- [133] D. Wijethunge, L. Zhang, and A. Du, Prediction of two-dimensional ferroelectric metal Mxenes, *J. Mater. Chem. C* **9**, 11343 (2021).
- [134] Q. Yang, M. Wu, and J. Li, Origin of two-dimensional vertical ferroelectricity in WTe_2 bilayer and multilayer, *J. Phys. Chem. Lett.* **9**, 7160 (2018).

- [135] L. Li and M. Wu, Binary compound bilayer and multilayer with vertical polarizations: Two-dimensional ferroelectrics, multiferroics, and nanogenerators, *ACS Nano* **11**, 6382 (2017).
- [136] D. K. Mann, A. M. Díez, J. Xu, O. I. Lebedev, Y. V. Kolen'ko, and M. Shatruk, Polar layered intermetallic LaCo_2P_2 as a water oxidation electrocatalyst, *ACS Appl. Mater. Interfaces* **14**, 14120 (2022).
- [137] D. Puggioni, G. Giovannetti, and J. M. Rondinelli, Polar metals as electrodes to suppress the critical-thickness limit in ferroelectric nanocapacitors, *J. Appl. Phys.* **124**, 174102 (2018).
- [138] J. M. Rondinelli and D. Puggioni, Noncentrosymmetric metal electrodes for ferroic device, Patent No. US-20180040711-A, United States (2017), <https://image-ppubs.uspto.gov/dirsearch-public/print/downloadPdf/20180040711>.
- [139] X. Liu, Y. Yang, T. Hu, G. Zhao, C. Chen, and W. Ren, Vertical ferroelectric switching by in-plane sliding of two-dimensional bilayer WTe_2 , *Nanoscale* **11**, 18575 (2019).
- [140] M. Moaied, M. M. A. Yajadda, and K. (Ken) Ostrikov, Quantum effects of nonlocal plasmons in epsilon-near-zero properties of a thin gold film slab, *Plasmonics* **10**, 1615 (2015).
- [141] S. Raza, T. Christensen, M. Wubs, S. I. Bozhevolnyi, and N. A. Mortensen, Nonlocal response in thin-film waveguides: Loss versus nonlocality and breaking of complementarity, *Phys. Rev. B* **88**, 115401 (2013).
- [142] H. Chalabi, D. Schoen, and M. L. Brongersma, Hot-electron photodetection with a plasmonic nanostripe antenna, *Nano Lett.* **14**, 1374 (2014).
- [143] B. Hou, L. Shen, H. Shi, R. Kapadia, and S. B. Cronin, Hot electron-driven photocatalytic water splitting, *Phys. Chem. Chem. Phys.* **19**, 2877 (2017).
- [144] M. L. Juan, R. Gordon, Y. Pang, F. Eftekhari, and R. Quidant, Self-induced back-action optical trapping of dielectric nanoparticles, *Nat. Phys.* **5**, 915 (2009).
- [145] M. L. Juan, M. Righni, and R. Quidant, Plasmon nano-optical tweezers, *Nat. Photonics* **5**, 349 (2011).
- [146] J. C. Ndukaife, A. V. Kildishev, A. G. A. Nnanna, V. M. Shalaev, S. T. Wereley, and A. Boltasseva, Long-range and rapid transport of individual nano-objects by a hybrid electrothermoplasmonic nanotweezer, *Nat. Nanotechnol.* **11**, 53 (2016).
- [147] D. N. Basov, R. D. Averitt, and D. Hsieh, Towards properties on demand in quantum materials, *Nat. Mater.* **16**, 1077 (2017).
- [148] Y. Wang, X. Liu, J. D. Burton, S. S. Jaswal, and E. Y. Tsymlal, Ferroelectric Instability Under Screened Coulomb Interactions, *Phys. Rev. Lett.* **109**, 247601 (2012).
- [149] V. F. Michel, T. Esswein, and N. A. Spaldin, Interplay between ferroelectricity and metallicity in BaTiO_3 , *J. Mater. Chem. C* **9**, 8640 (2021).
- [150] J. Serre and A. Ghazali, From band tailing to impurity-band formation and discussion of localization in doped semiconductors: A multiple-scattering approach, *Phys. Rev. B* **28**, 4704 (1983).
- [151] A. L. Efros, N. V. Lien, and B. I. Shklovskii, Impurity band structure in lightly doped semiconductors, *J. Phys. C: Solid State Phys.* **12**, 1869 (1979).
- [152] E. Pastor, M. Sachs, S. Selim, J. R. Durrant, A. A. Bakulin, and A. Walsh, Electronic defects in metal oxide photocatalysts, *Nat. Rev. Mater.* **7**, 503 (2022).
- [153] S. Raghavan, J. Y. Zhang, O. F. Shoron, and S. Stemmer, Probing the metal-insulator transition in BaTiO_3 by electrostatic doping, *Phys. Rev. Lett.* **117**, 037602 (2016).
- [154] K. Page, T. Kolodiaznyi, T. Proffen, A. K. Cheetham, and R. Seshadri, Local structural origins of the distinct electronic properties of Nb-substituted SrTiO_3 and BaTiO_3 , *Phys. Rev. Lett.* **101**, 205502 (2008).
- [155] A. Walsh and A. Zunger, Instilling defect tolerance in new compounds, *Nat. Mater.* **16**, 964 (2017).
- [156] A. Marcelli, M. Coreno, M. Stredansky, W. Xu, C. Zou, L. Fan, W. Chu, S. Wei, A. Cossaro, A. Ricci, A. Bianconi, and A. D'Elia, Nanoscale phase separation and lattice complexity in VO_2 : The metal-insulator transition investigated by XANES via auger electron yield at the vanadium L_{23} -edge and resonant photoemission, *Condens. Matter* **2**, 38 (2017).
- [157] S. Salmani-Rezaie, K. Ahadi, and S. Stemmer, Polar nanodomains in a ferroelectric superconductor, *Nano Lett.* **20**, 6542 (2020).